Seabed properties and geohazards across the Arctic Ocean

A Polar Connect desktop study within the Northern EU Gateways to investigate seabed conditions for the installation of a communication cable across the Arctic Ocean

Martin Jakobsson and Vicent Doñate

Department of Geological Sciences, Stockholm University, Stockholm, Sweden

1. Introduction and task

This desktop study has been requested by the Swedish Research Council-SUNET and is part of the Northern European initiative Polar Connect under the Connecting Europe Facility2 (CEF-2 program) funded project Northern EU Gateways. The overarching goal of Polar Connect is to explore the feasibility of connecting the Nordic countries to Asia using fiber optic cables via the Arctic Ocean. Specifically, this desktop study focuses on **seabed properties and geohazards** in the central Arctic Ocean, **sea-ice covered** segment of a potential route, which would connect Svalbard, Bering Strait and Japan and Korea (Fig. 1). The perennial Arctic Ocean sea-ice cover reaches its annual minimum extent around mid-September. A common long-term reference is the September median sea-ice extent from 1991 to 2010, which extends from north of Svalbard at about 80°N to approximately 73°N, north of the Bering Strait (Fig. 1). Consequently, this study investigates seabed properties and viable cable routes from the continental shelf of Svalbard off New Ålesund to north of the Bering Strait. As sea-ice conditions will greatly affect the logistical challenges of a cable installation on the seafloor, they were considered in addition to seabed properties and geohazards for two of the four optional routes (R1 to R4) in this study. In general, the sea-ice conditions pose more challenges for icebreaker operations on the northern Greenland and Canadian Arctic Archipelago side of the central Arctic Ocean compared to a route closer to the North Pole. (Fig. 2).

The following is included in the study:

1. An analysis of existing seabed data to identify areas based on seabed properties and geohazards to evaluate their suitability for fiber optic cables.
2. Identification of areas relevant to Polar Connect where seabed data is lacking or are of poor quality, limiting the assessment of suitability for fiber optic cables.
3. Recommendations for potential cable routes based on available data, along with suggestions for supplementary seabed surveys.

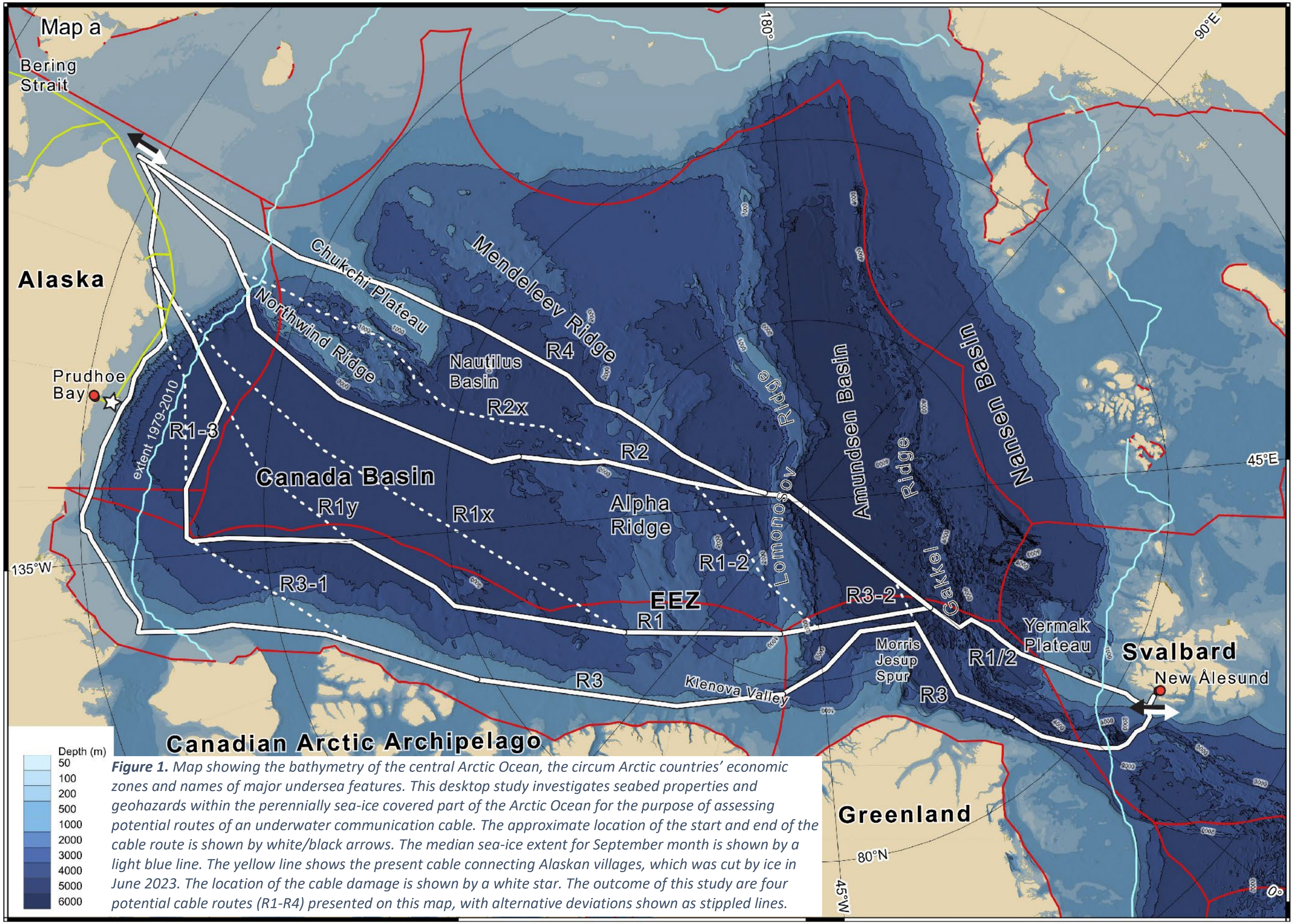

Figure 1. *Map showing the bathymetry of the central Arctic Ocean, the circum Arctic countries' economic zones and names of major undersea features. This desktop study investigates seabed properties and geohazards within the perennially sea-ice covered part of the Arctic Ocean for the purpose of assessing potential routes of an underwater communication cable. The approximate location of the start and end of the cable route is shown by white/black arrows. The median sea-ice extent for September month is shown by a light blue line. The yellow line shows the present cable connecting Alaskan villages, which was cut by ice in June 2023. The location of the cable damage is shown by a white star. The outcome of this study are four potential cable routes (R1-R4) presented on this map, with alternative deviations shown as stippled lines.*

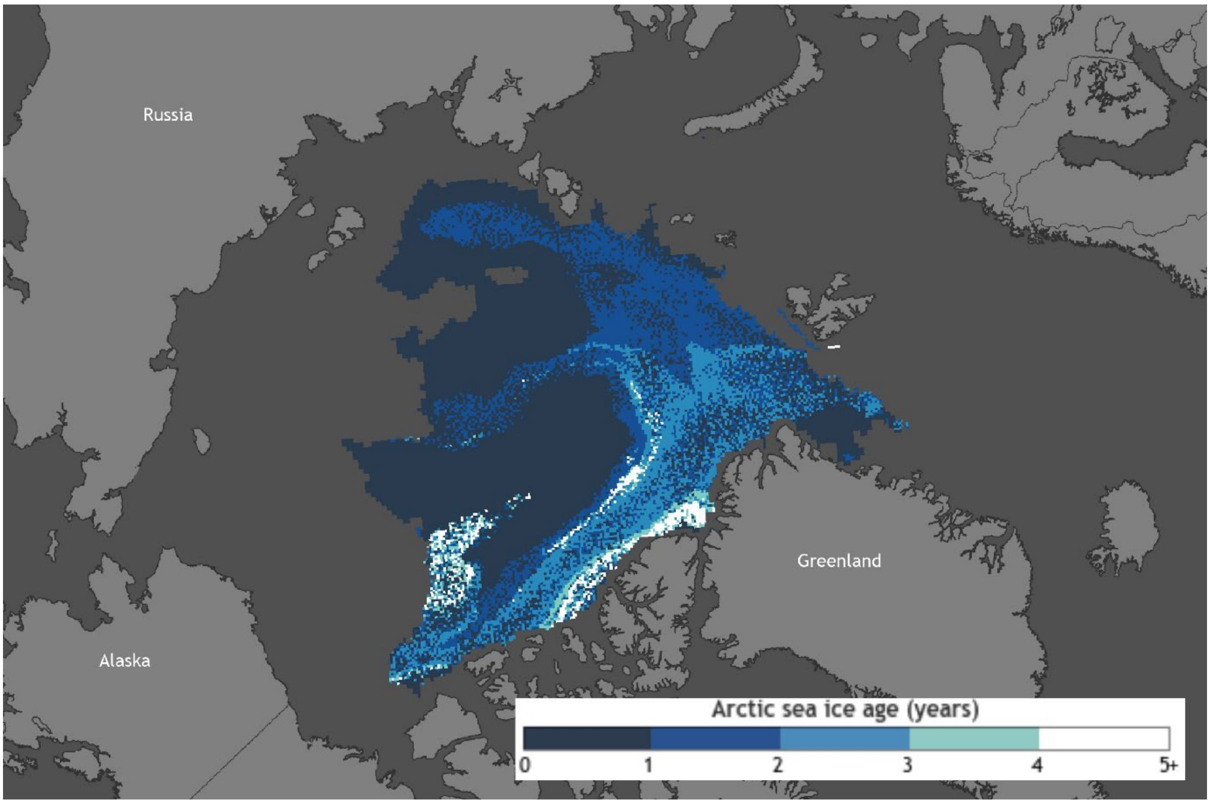

Figure 2. *Map of sea-ice age in September 10, 2023, based on National Snow and Ice Data Center's (NSIDC) Quicklook Arctic Weekly EASE-Grid sea ice age, version 1. Older sea ice is thicker and more difficult for icebreakers to operate in, compared with conditions in younger sea ice. The map indicates that more difficult conditions persist north of Greenland and the Canadian Arctic Archipelago.*

Seabed properties is here taken to include bathymetric and geologic properties, such as seafloor depth, slope and roughness and seabed sediment/rock composition as well as ongoing/past processes. These properties are further elaborated below and subsequently evaluated with respect to seabed geohazards affecting a cable installation. Although the study is primarily focused on identifying suitable routes within the Exclusive Economic Zones (EEZ) of Svalbard/Norway, Greenland/Denmark, Canada, and the United States in the Arctic Ocean, we have also explored potential routes outside of these zones, considering the fact that sea-ice conditions are more difficult for icebreaker operations along the northern Greenland and Canadian Arctic Archipelago sector of the central Arctic Ocean (Fig. 2).

Disclaimer

The authors of this report cannot be held responsible for any potential erroneous interpretations of the data presented herein or the proposed cable routes.

Premises

This desktop study is based on openly available data and the points below are considered when selecting potential routes. Points listed within brackets are commonly included in desktop studies of cable routes, but are not included here as they were not part of the assignment.

What to Avoid:

1. **Steep underwater slopes and rough seafloor**: Steep areas can be more prone to landslides and underwater geological activities that can damage the cable. Rough seafloor may also impose hazards to a cable installation.

2. **Submarine canyons**: Submarine canyons, which are deep, relatively narrow, are often subject to strong currents and sediment transport.
3. **Volcanic or seismically active areas**: Submarine volcanic eruptions and earthquakes can disrupt the cable and its infrastructure.
4. **Areas prone to dynamic seabed changes**: Active sedimentary or tectonic processes that reshape, lower or raise the seabed should be avoided as they could cause excess burial, freespans (cable not in contact with the seafloor), or stresses along the cable length. Examples include fluid escape, seabed faulting, processes related to subsea permafrost, or sediment mass transport.
5. **Areas prone to ice scouring**: Icebergs and sea-ice pressure ridges can pose a significant threat to underwater cables if they ground on the seafloor.
6. **(Sensitive habitats)***:* This criterion was not part of the assignment and is therefore not accounted for in this desktop study. Consequently, sensitive habitats have not been considered for the proposed cable routes.
7. **(Areas with demersal fishing activity)***:* Cable routes are commonly avoiding areas of heavy fishing activity, as trawlers and their gear can damage cables. Commercial demersal trawling is carried out along the west coast of Svalbard up to approximately 80°N and in the Bering Sea. However, considering fishing activity when analyzing the seabed conditions for potential cable routes is beyond the assigned task of this desktop study.
8. **(Shipping traffic)**: Major shipping lanes and congested maritime areas are usually avoided to reduce the risk of accidental cable damage from ship anchors and other maritime activities. As this study concerns the high Arctic, there are no areas of heavy marine traffic. Most trafficked is the Bering Strait.

What to Prefer:

a. **Flat or gently sloping and smooth seafloor**: Routes with relatively flat or gently sloping seafloor terrain reduce the risk of cable exposure and damage due to underwater disturbances.

b. **Deep water**: Deeper waters are generally less affected by surface waves and currents, and away from ice scouring, providing better protection for a cable.

c. **Geologically stable areas**: Regions of geological stability minimize the risk of cable damage from underwater disturbances.

d. **(Minimal environmental impact)**: Preferable cable routes are those with minimal environmental impact, especially in ecologically sensitive areas. However, conducting an environmental impact assessment is not one of the assigned tasks for this desktop study.

e. **(Legal compliance)**: Ensure compliance with international and regional laws and regulations governing cable placement. This may involve obtaining permits and consulting with relevant authorities, which is not part of the assignment of this desktop study.

f. **(Maintenance Access)**: Planning for regular maintenance and repair access points along the cable route is not part of the assignment and is therefore not considered.

g. **(Security Measures)**: Addressing security measures to protect the cable infrastructure from unauthorized access or tampering is not part of the assignment and not included in this desktop study.

The desktop study employs the concept of compiling a "geocost map" as described in *American Bureau of Shipping* [2016], although with modifications to suit the available data and our region of interest. Geohazards listed in points 1-5 above are evaluated in terms of geocosts using available data (e.g., bathymetry and sub-bottom profiles) and information from previous studies. The results are summarized in a geocost map that guides route selection by taking the least-geocost pathway. The methodology applied is further described in the Data and Methods section below. This geocost approach is common in desktop studies investigating routes for pipelines, communication cables, and similar applications, not limited to the marine realm [*Iqbal et al.*, 2006].

This report includes two appendices that supports our assessment of seabed properties:

- Appendix 1: Geological interpretations of sub-bottom profiles and assignment of acoustic facies
- Appendix 2: Ice scouring on the seabed of the Arctic Ocean

This report has been prepared in collaboration with Kai Boggild, Geological Survey of Canada, who led the compilation of geohazard examples across the Arctic Ocean, which will be published in a Geological Survey of Canada Open-File report [*Boggild and Jakobsson*, in prep]. We base a great deal of our conclusions on the results presented in the Open-File report.

2. Data and methods

2.1 Bathymetry

The seafloor bathymetry and derived products, such as slope and measures of roughness, are based on the International Bathymetric Chart of the Arctic Ocean (IBCAO) gridded Digital Bathymetric Model (DBM) [*Jakobsson et al.*, 2020]. This DBM has a grid-cell size of 200×200 m on a Polar Stereographic projection, true scale 75°N. Here we use IBCAO version 4.2.13, compiled in September 2023 (Fig. 1), with the depth data sources detailed in Figure 4 (Map b). For the focused analysis of route selection, a specific DBM with a grid-cell size of 100×100 m was generated (Fig. 4; Map c). This model is assembled using a near neighbor algorithm exclusively from multibeam bathymetry and dense single-beam data, derived from the IBCAO database. This implies that gaps between bathymetric survey lines are not interpolated, which has the advantage of showing where depth data is supporting the route selection and where data coverage is lacking.

Seafloor slope and roughness have been derived from IBCAO using the algorithms available within QGIS [*QGIS Development Team*, 2023]. Slope is the first derivative of bathymetry and represents the rate of depth change of the bathymetry (Fig. 5; Map d). Roughness is a measure of the irregularity of the seafloor as expressed by the largest difference between a grid cell-center and its neighbors.

2.2 Seafloor and sub-bottom geology

A regional assessment of surficial geology in the central Arctic Ocean region is based on maps of interpreted acoustic facies derived from sub-bottom profiler data compiled through the international collaborative project "IBCAO Geology" [*Boggild et al.*, 2018; *D.C. Mosher et al.*, 2015; *Van der Krogt*, 2018]. The approach used to develop these maps classifies sub-bottom profiler data into acoustic facies according to the characteristics of the seafloor echo and sub-bottom reflections. Geological interpretations of these facies are subsequently made by combining them with physiography and sediment core information where available [*Damuth*, 1980]. The classification scheme of *Boggild et* *al.* [2018] is shown in Table 1. These facies are organized into (a) principal categories (Table 1) and (b) compound facies (Table 2), used to describe areas where more than one principal facies are recognized in various stratigraphic relationships (e.g., truncating, interbedded with, over). Generalized geological interpretations of each acoustic facies and compound facies are shown in Tables 1 and 2 according to the typical setting where they are located. In addition to the facies distributions mapped in the Amerasia and Amundsen basins by [*Boggild et al.*, 2023]; *Boggild et al.* [2018], facies have been mapped in this study using sub-bottom profiles collected with Swedish icebreaker (IB) *Oden*, primarily in the Eurasia Basin. Interpretations of selected sub-bottom profiles are shown in Appendix 1.

2.3 Seismicity

The seismicity in the Arctic Ocean is visualized using the database of earthquakes from the International Seismological Centre's (ISC) Global Instrumental Earthquake Catalogue (GEM) (www.isc.ac.uk/). The ISC-GEM stores earthquakes with magnitude 5.5 or higher plus continental events of significance with lower magnitudes. Here version 10 published 21 March 2023 is used, which contains earthquakes between 1904 and 2019. The first ISC-GEM was published by *Storchak et al.* [2013]. Earthquakes from ISC-GEM in the central Arctic Ocean are shown on the geocost maps (see below).

2.4 Geohazards and geocost

Geohazards are categorized as geometric and process hazards (Tables 3 and 4). Geometric hazards relate to static seabed properties, including steep slopes, ridges, or rough seafloor resulting from, for example, exposed bedrock, ice scouring, and mass-waste deposits. Process hazards involve dynamic geological or oceanographic processes, such as ice scouring, mass wasting, strong bottom currents, and sediment transport. Figure 3 illustrates common geological and oceanographic hazards for underwater installations. We assigned hazard levels of 1-3 to geometric hazards and 1-6 to process hazards, with higher ranks indicating greater risk to underwater installations. These arbitrary values are then considered equivalent to geocosts.

The hazard levels assigned in Tables 3 and 4 are inferred based on the acoustic facies interpretation of the sub-bottom profiles (Appendix 1). These hazard levels are subsequently used in our geocost evaluation, along with seafloor slope derived from the IBCAO bathymetry. The seafloor slope has been assigned hazard levels (geocost) values in Table 5. While seafloor roughness is an important parameter, we did not include it in the final geocost calculation as it does not significantly add to the slope parameter. Moreover, roughness is already considered in the hazard levels prescribed to the interpreted sub-bottom profiles (Table 3). The final geocost was calculated using the following equation:

$$Geocost = \frac{GH+PH+SH}{3}, \quad (1)$$

where *GH* is the assigned level of geometric hazards (Table 3), *PH* the assigned hazard level of process hazards (Table 4) and *SH* the slope hazard level following Table 5. Process hazards are given a higher weight in Equation 1 because *PH* is assigned values 1-6, compared to 1-3 for *GH* and *SH*. This decision is motivated by the recognition that process (or dynamic) hazards frequently present more significant challenges than geometric hazards. Furthermore, slope (*SH*) is also included in the Equation, which is a geometric hazard adding to *GH*. When evaluating the seabed properties and geohazards relevant for a cable route, we have in addition to the geocost derived from Equation 1, visually investigated the seafloor bathymetry, included hazards from seismicity (Figs. 7), and hazards from ice scouring by sea-ice ridges and icebergs (Appendix 2).

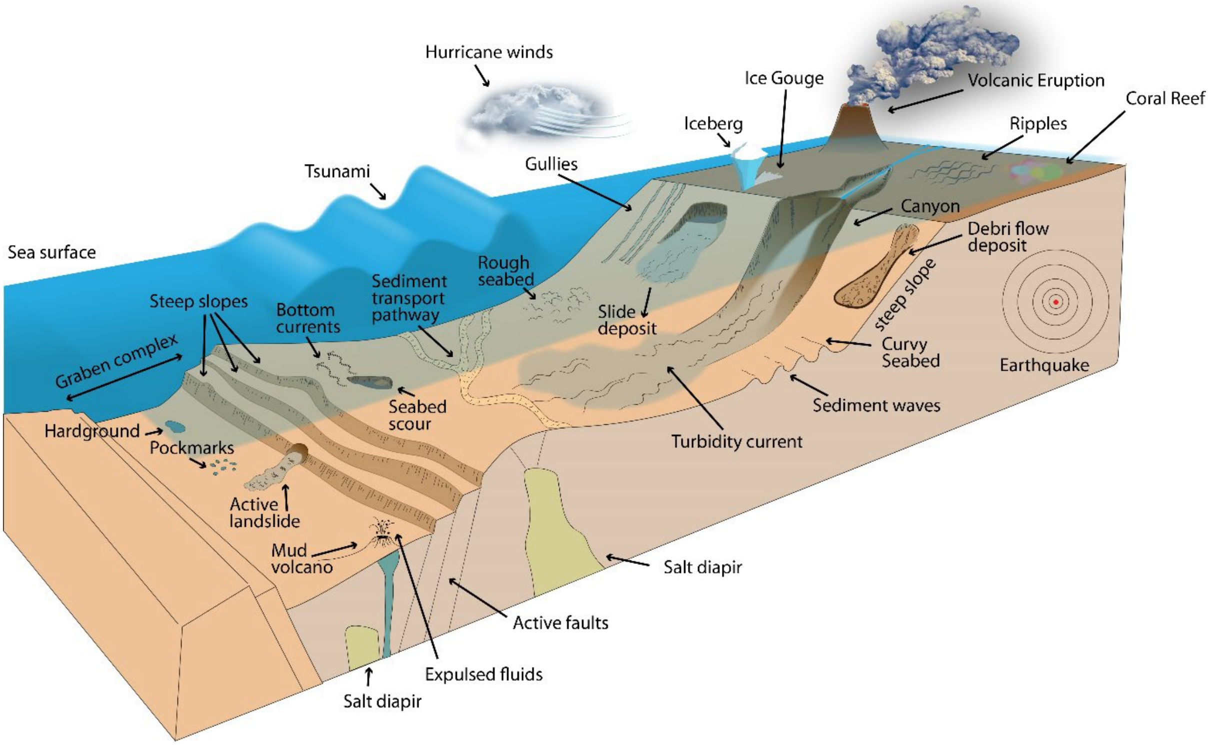

Figure 3. *Geohazards commonly accounted for when planning underwater installations. The figure modified from the American Bureau of Shipping [2016].*

Table 1. *Acoustic facies and their geological interpretation.*

Category	Facies	Example	Description	General geologic interpretation
Chaotic/Irregular Seafloor	1a	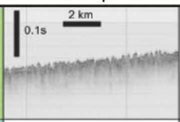	Chaotic bottom echo with amorphous or transparent sub-bottom reflections.	**Shelf**: Ice-scoured and turbated sediment **Shelf break**: Slump/mass transport deposit (MTD) **Slope/Aysal Plain**: MTD
	2a	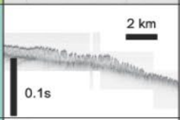	Scoured bottom echo with amorphous or transparent subbottom and semi-parallel incoherent reflections.	**Shelf/Shelf Break**: Ice-scoured sediment with turbated upper layer.
	2b	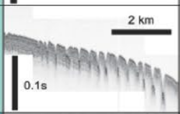	Semi-parallel coherent reflections interrupted by troughs at the seafloor surface.	**Shelf/Shelf Break**: Ice-scoured bedded sediments minimal or no turbation.
	3a	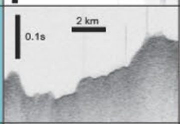	High amplitude, irregular bottom echo with amorphous subbottom reflections.	**Shelf**: Eroded surface **Slope**: Eroded surface, exposed bedrock, MTD or channel thalweg **Abyssal Plain**: Exposed bedrock (seamount), channel thalweg
	3b	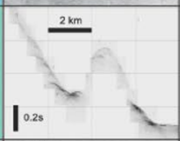	Varying amplitude, broad or one-sided hyperbolic bottom echo with no subbottom reflections. Occur on steep bathymetric gradients. Hyperbolae 1-2 km in width.	Fault scarp or basement structure
	4a	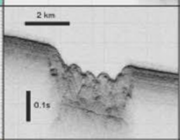	Overlapping narrow hyperbolic reflections with absent or amorphous subbottom reflections occurring on flat or gently sloping seafloor. Hyperbolae 0.1-1.0 km in width.	**Shelf**: Ice-push, ice-scour **Slope**: Slump/MTD **Abyssal Plain**: MTD
Smooth Seafloor/ Transparent	5a	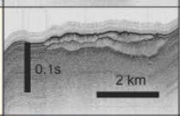	Smooth bottom echo with incoherent transparent lens-shaped deposit(s).	**Shelf**: Diamict **Slope**: Debris flow, MTD
	6a	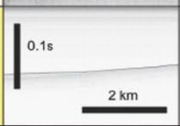	High amplitude, smooth bottom echo with acoustically transparent subbottom.	**Shelf**: Undisturbed deglacial and post-glacial deposits **Slope**: Channel lag deposits part of MTD
Coherent subbottom reflections = Bedded/Laminated	7a	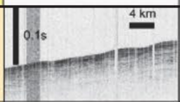	Smooth undulating, coherent parallel to subparallel reflections. Reflections pinch out, diverge, or vary in amplitude laterally.	**Shelf Break**: Current-influenced glaciomarine and post-glacial deposits **Slope**: Mixed turbidites/hemipelagites, fan **Abyssal Plain**: Undulating turbidites or contourites
	7b	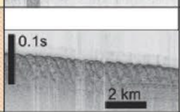	Smooth, wavy coherent parallel to subparallel reflections with sediment waves. Sediment waves defined by dipping planes of pinching reflections.	**Slope**: Fan sediments, levee sediments related to deep-sea channels
	7c	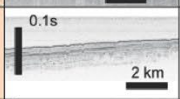	Smooth bottom echo with coherent parallel reflections that experience blanking at depth.	**Shelf/Shelf Break**: Permafrost sediments, glacio-marine sedimenets with buried syn-sedimentary ice scours, or gas if complete blanking.
	7d	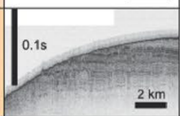	High amplitude smooth bottom echo truncating coherent, semi-parallel subbottom reflections. May experience blanking at depth.	**Shelf**: Eroded glaciomarine / periglacial sediments. Blanking due to gas, buried margin wedges, buried ice scours
	7e	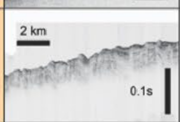	Rugose bottom echo with semi-coherent contorted parallel/sub-parallel and amorphous subbottom reflections	**Slope**: Deformed sediments, MTD, or fan deposits with small-scale sediment waves.
	7f	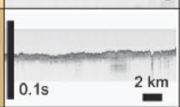	Chaotic bottom echo truncating, coherent semi-parallel reflections.	**Shelf**: Eroded preglacial / glaciomarine sediments
	8a	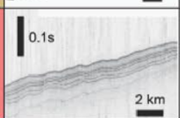	Smooth bottom echo with coherent parallel to sub-parallel reflections that mimic bathymetry. Subbottom reflections maintain a consistent amplitude laterally.	**Shelf**: Laminated glaciomarine / Holocene hemipelagic drape deposits **Slope**: Hemipelagic drape, mixed fan sediments
	9a	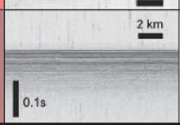	Smooth, flat-lying, coherent parallel reflections. Reflections typically onlap neighboring facies or structural highs. Reflections may thicken towards depocenter.	**Abyssal plain**: Flat-lying turbidites and interbedded hemi-pelagites

Table 2. *Acoustic compound facies and their geological interpretation.*

Category	Facies	Example	Description	General geologic interpretation
Compound Facies	1a over 6a	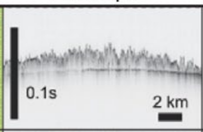	Chaotic bottom echo with amorphous/transparent subbottom reflections overlying high amplitude smooth echo with amorphous/transparent subbottom.	**Shelf:** Ice-scoured sediment, till, undifferentiated glacimarine iceberg turbate
	1a over 1a	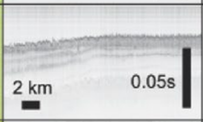	Chaotic bottom echo with amorphous/transparent subbottom reflections overlying chaotic subbottom reflections.	**Shelf:** Stacked ice-scoured/till deposits/till tongues
	1a truncating 8a	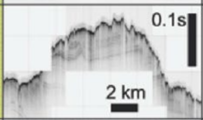	Chaotic bottom echo with amorphous subbottom reflections overlying chaotic subbottom reflections.	**Shelf:** Ice-scoured sediment/diamict unconformably overlying older stratified sediments
	5a over 8a	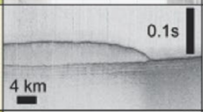	Smooth bottom echo with incoherent transparent wedge deposits overlying coherent parallel/sub-parallel subbottom reflections.	Debris flow/MTD/diamict over stratified sediment (e.g. hemipelagic/turbidites/glacimarine)
	6a over 1a	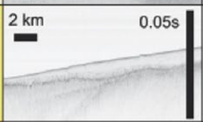	Smooth bottom echo with amorphous subbottom overlying chaotic subbottom reflection(s).	**Shelf:** Undisturbed post/de-glacial sediments over chaotic surface
	8a interbedded with 5a	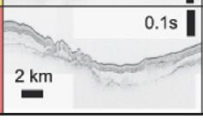	Smooth bottom echo with draping coherent subbottom reflections interbedded with transparent wedge shaped deposits.	**Slope:** Hemipelagic drape interbedded with MTDs/debris flows

Table 3. *Geometric hazards ranked in terms of hazard level from 1 to 3.*

Hazard level	Inclusions
3 - Highest	- Rough seafloor, commonly due to exposed bedrock, escarpments, iceberg/sea ice scours, mass wasting or strong bottom currents. - Complex seabed in shelf areas with likelihood of variable sub-bottom conditions for cable burial. For example, a heavily ice scoured seafloor is often underlaid by a diamict that may contain coarse sediments, even boulders, that could affect trenching operations for cable burial.
2 - Moderate	- Generally smooth, partly flat, but commonly undulating seafloor
1 - Lowest	- Generally smooth, flat to gently sloping bottom

Table 4. *Process hazards ranked in terms of hazard level from 1 to 6.*

Hazard Level	Description	Inclusions
6 – Ongoing hazard	Areas most likely to be affected by ongoing dynamic geological or oceanographic processes. Surficial morphological features formed by continuous processes (e.g., pockmarks) are assumed recent without evidence to the contrary.	- Modern ice scour - Volcanic hazards (e.g. Gakkel Ridge) - Seismic hazards (e.g., Gakkel Ridge) - Fluid escape features (mud volcanos, pockmarks) - Active thermokarst processes (marine pingos, pingo-like features) - Sediment pathways (canyons and channels) - Seabed erosion by currents - High angle escarpments, either due to headwall area of mass failures, faulting, or bedrock
5 - Recent hazards	Areas shown to be subject to slope instability on centennial - millennial timescales or longer. Since ages of slope failure vary widely in the study area and mostly lack constraints, recent Holocene failures (e.g., Beaufort Slope) and earlier slope failures (e.g., Hinlopen Slide, glacial debris) are considered together at the same hazard level.	- Submarine landslides (mass transport deposits)
4 - Recent hazards	Areas downslope of sedimentary sources (e.g., slope failures, sediment conduits) affected by episodic currents.	- Turbidites and contourites
3 - Relatively stable (some current influence)	Morphologically stable areas subject to shallow currents.	- Deglacial muds on shelf with minor current sculpted features
2 - Recently stable (complex subsurface)	Areas with complex subsurface and morphology produced by processes that are no longer active.	- Ancient ice-scour (deep)
1 - Recently stable (simple subsurface)	Areas lacking evidence of dynamic processes.	- Hemipelagic sedimentation, e.g. abyssal plains

Table 5. *Hazard levels assigned to seabed slope.*

Hazard level	Seabed slope angle (°)
3	>10
2	5 - 10
1	0 - 5

3. Results

This section outlines identified geological hazards along potential submarine cable routes, originating from the Svalbard continental shelf off New Ålesund. These routes traverse either the Fram Strait or, as an alternative, the Yermak Plateau, and further extend through the Eurasia and Amerasia basins, concluding north of the Bering Strait where the cable route assessment ends. To facilitate a comprehensive description of potential cable routes, the assessment is divided into geographic sections. The foundation for this assessment is built upon the geocost analysis, along with all compiled information found in Appendices 1-2 and the Open File report [Boggild and Jakobsson, in prep.]. Modern depths of iceberg scours (<60 m in the Canadian-US Arctic and <125 m around Svalbard, Appendix 2) have been paid specific attention in addition to their influence on the geocost map from analyses of sub-bottom profiles. Four main alternatives are given:

- **Route 1 (R1),** entirely inside the EEZs of Svalbard/Norway, Greenland/Denmark, Canada, and the United States.
- **Route 2 (R2),** partly outside of the EEZs of Greenland, Canada and the United States to avoid the most difficult sea-ice conditions north of Greenland and the Canadian Arctic Archipelago.
- **Route 3 (R3),** entirely inside the EEZs of Svalbard/Norway, Greenland/Denmark, Canada, and the United States and including the shallow continental shelves of the western Arctic (Canadian Arctic Archipelago, Beaufort and Alaskan shelves).
- **Route 4 (R4),** a lowest cost alternative considering sea-ice conditions and shortest distance across the central Arctic Ocean.

3.1. Svalbard Continental Shelf – Yermak Plateau – Fram Strait

Two options for the first section of the cable route are considered: (a) Northward from New Ålesund, along the Svalbard continental shelf and onto the Yermak Plateau, (b) Westward from New Ålesund, across the Fram Strait and then northward. The former option is partly poorly mapped implying that there may be hazards we are not aware of, for example mass wasting along the Yermak Plateau slope (Fig. 4). The two routes (R1/R2) are shown in Figure 7.

3.1.1 Dynamic Hazards:

The route heading north of New Ålesund runs along the continental shelf due north at depths >125 m to avoid modern iceberg scouring [*J.A. Dowdeswell and Forsberg*, 1992] (Fig. 7, Appendix 2). We call this Route 1/2 as it splits into either Route 1 or 2 just before the outer limit of the EEZ of Greenland/Danmark north of Morris Jesup Spur. Large ancient iceberg/shelf scours are mapped at the Yermak Plateau along the proposed cable route (R1/2), although these are not classified as modern dynamic hazards as they were produced during glacial periods >15 000 years ago [*J. A. Dowdeswell et al.*, 2010; *Jakobsson et al.*, 2016] (Fig. 8). Cable route R1/2 reaches the north-western slope of the Yermak Plateau, where it transects the Nansen Basin to reach the Gakkel Ridge. The second option (R3), running west from New Ålesund, implies transecting down the western Svalbard continental shelf slope to water depths >2000 m (Fig. 7). The bathymetry of R3 is mapped with multibeam and there are no clear signs of fresh mass wasting at the seafloor along this proposed cable route, suggesting recently stable slopes. Potential preconditioning factors for slope instability exist however along this margin. In the subsurface, sub-bottom profiles show debris flows along the upper slope that are of glacial origin and related to glacial activity during the Last Glacial Maximum (LGM) [*Wiberg et al.*, 2022]. These glacial debris flows are interbedded with glacimarine and plumite sediments [thin-bedded sand/mud couplets typical in turbidite systems, *Hesse et al.*, 1997] with varying physical properties [*R. G. Lucchi et al.*, 2013; *Wiberg et al.*, 2022], which can give rise to weak layers along formerly glaciated margins [*Gatter et al.*, 2021]. Downslope of buried glacial debris flow features, route R3 passes just south of mapped pockmark features along Vestnesa Ridge, where active gas venting is observed at pockmarks [*Bünz et al.*, 2012; *Hustoft et al.*, 2009]. While the proposed route mostly avoids these features, fluid flow and related sedimentary faulting have a localized effect on nearby seabed stability [*Elger et al.*, 2018; *Plaza-Faverola et al.*, 2023].

The Molloy Hole and Molloy Fracture Zone to the south and Spitsbergen Fracture Zone to the north, is a region of considerable seismicity (Fig. 7). In R3, the cable passes the Fram Strait in an area with smooth seafloor north of where numerous earthquakes are catalogued in ISC-GEM, of which two along the Molloy Fracture Zone have recorded magnitudes of >6. R3 subsequently runs along the western side of the Gakkel Ridge to north of Morris Jesup Spur. Unavoidably, R3 passes not too far from the Spitsbergen Fracture Zone, unless it is pulled up on the Greenland continental shelf – implying other hazards. The seafloor is for the most part unmapped along this route, implying that we cannot assess geohazards (Figs. 4, 7).

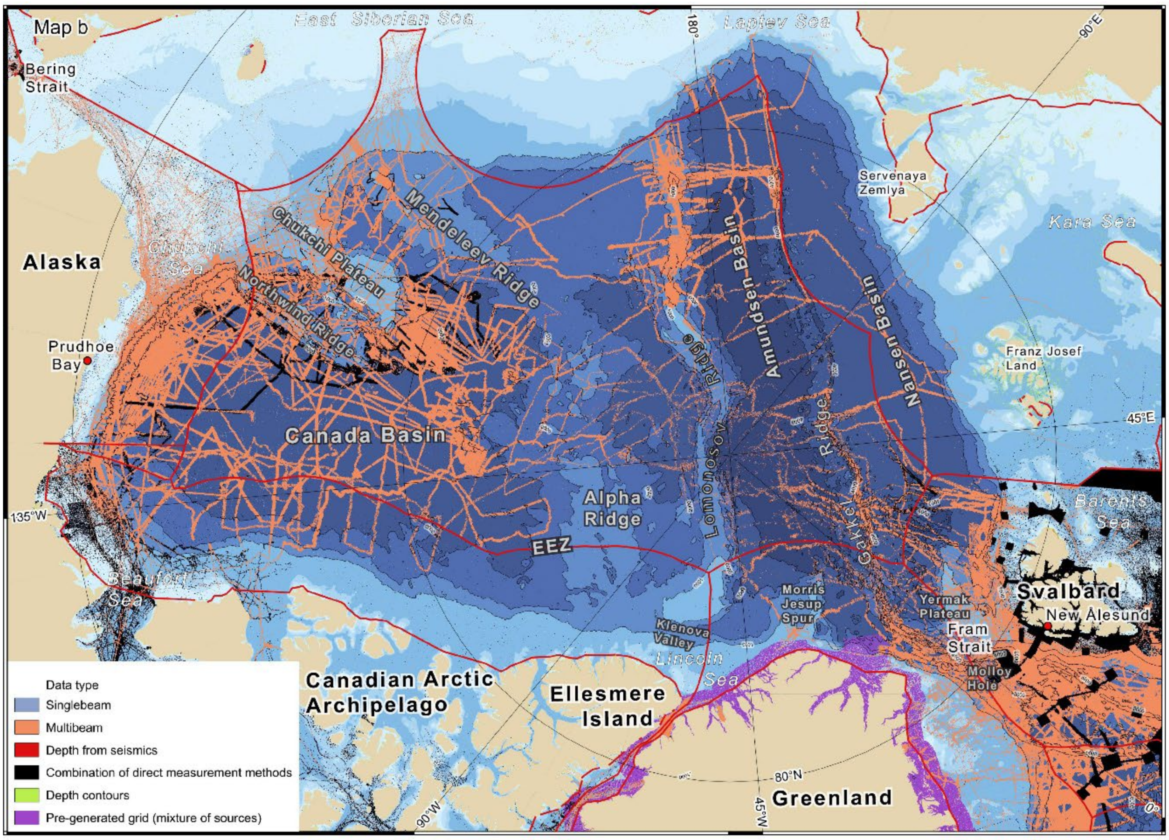

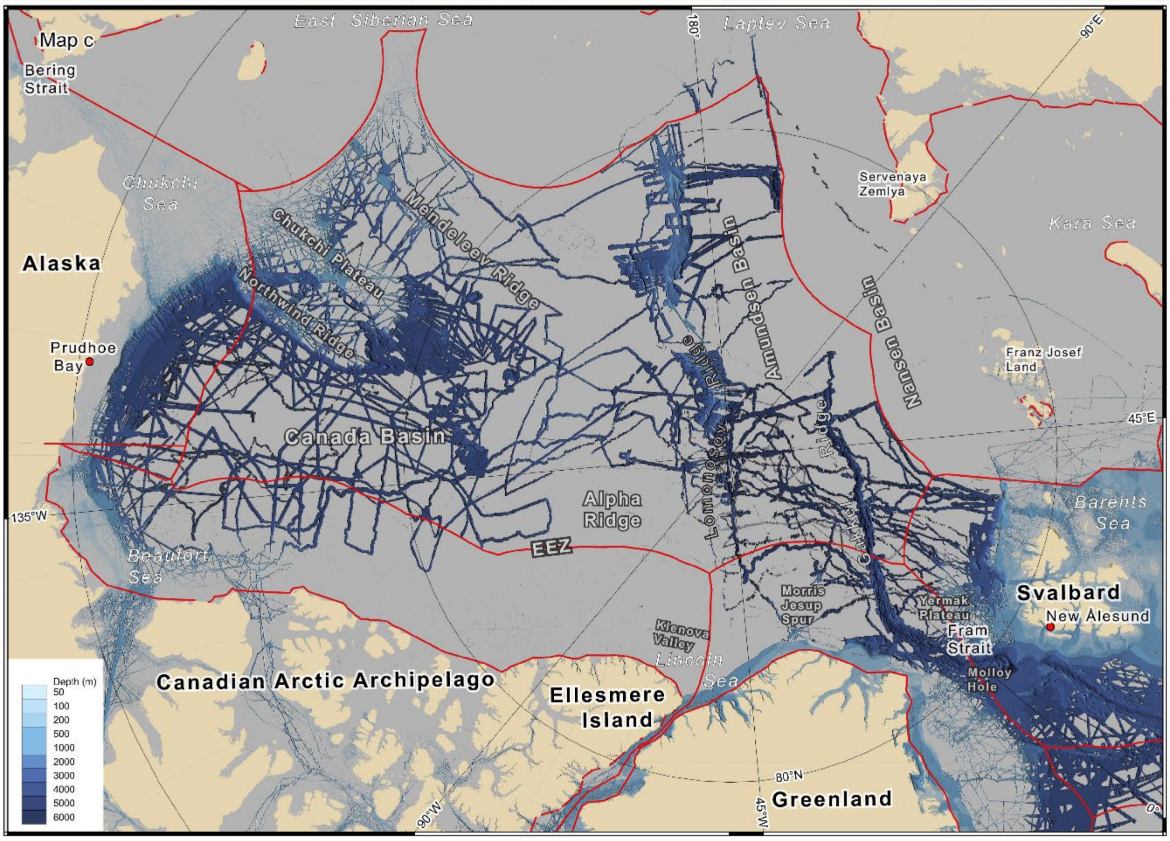

Figure 4. Map b: *Bathymetric source data of IBCAO Version 4.2.13.* ***Map c:*** *Bathymetry compiled using a near neighbour algorithm on multibeam bathymetry and dense single beam data only. The gray areas are poorly mapped.*

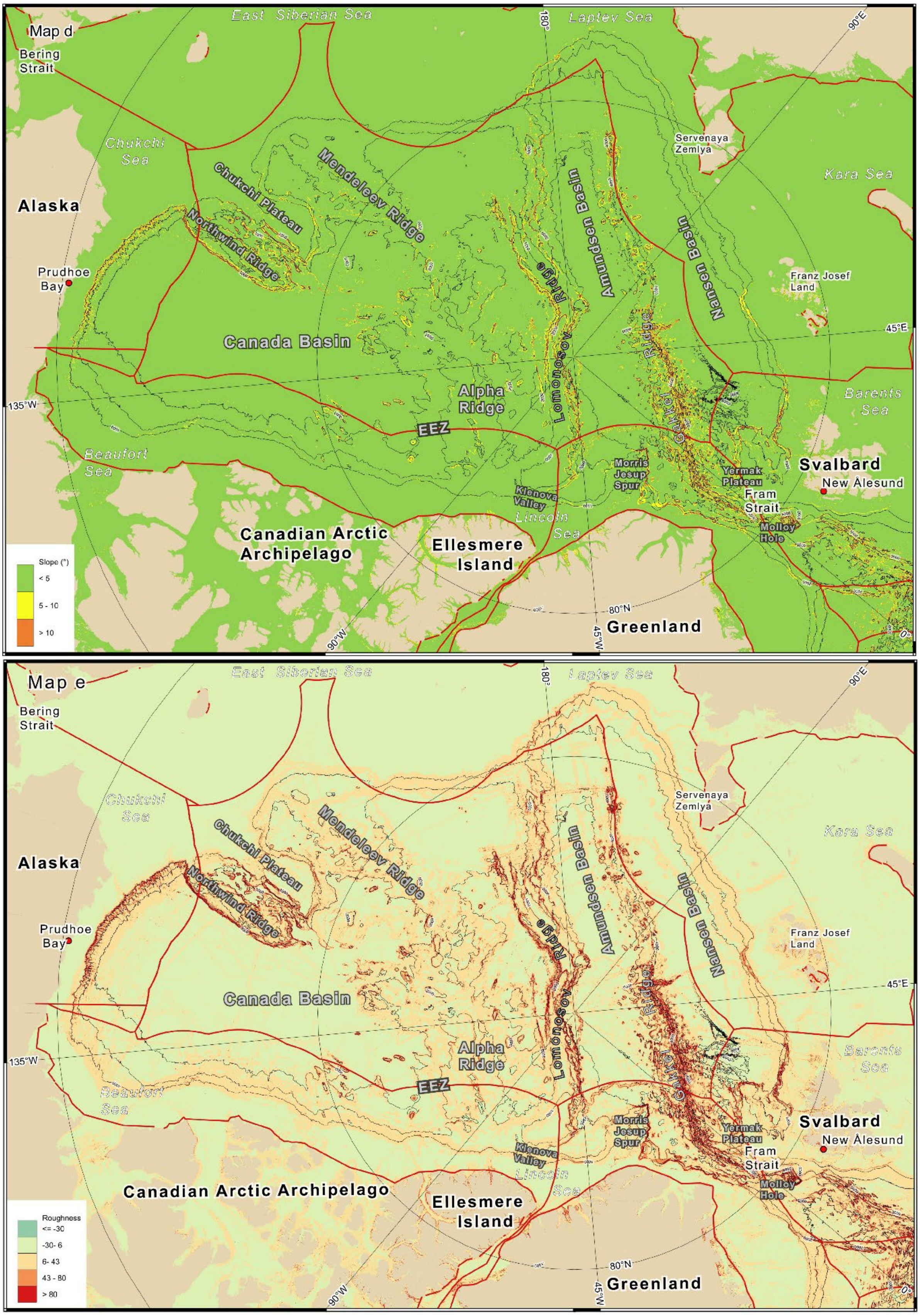

Figure 5. ***Map d:*** *Slope.* ***Map e:*** *Roughness.*

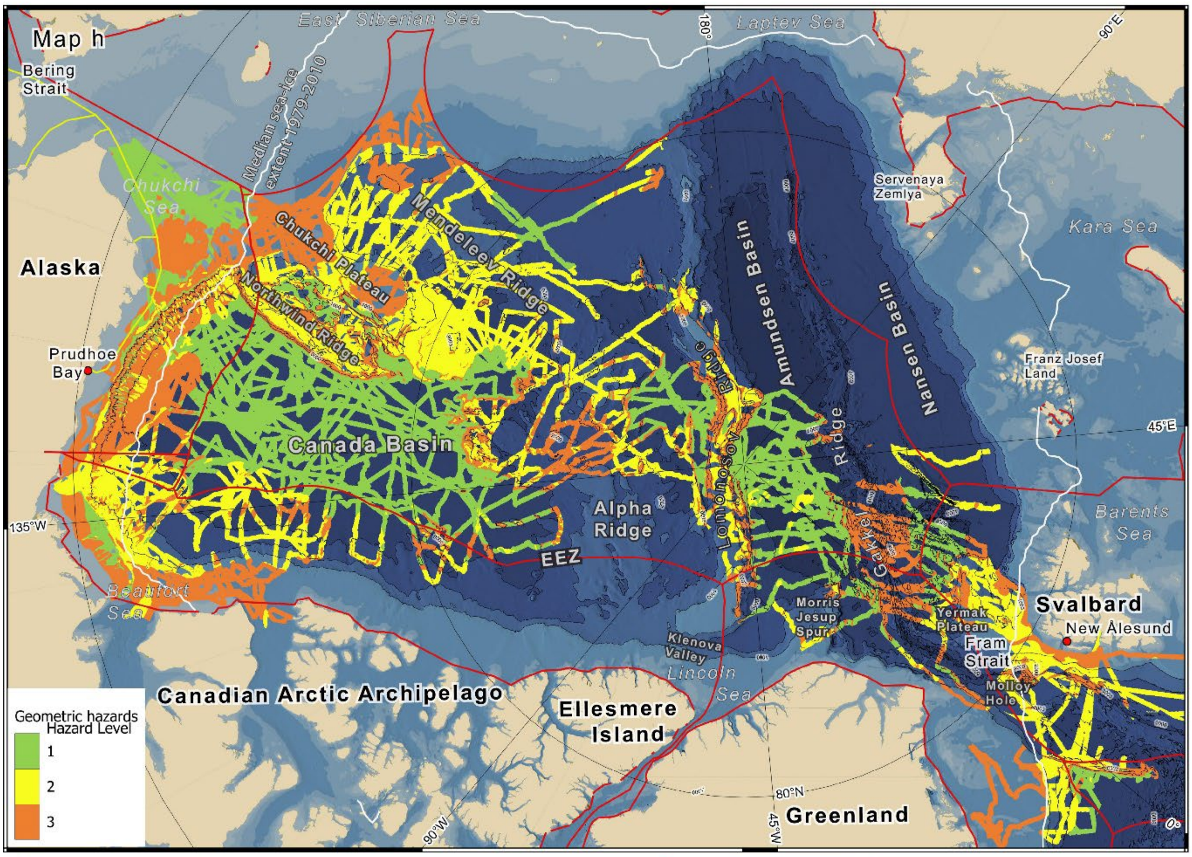

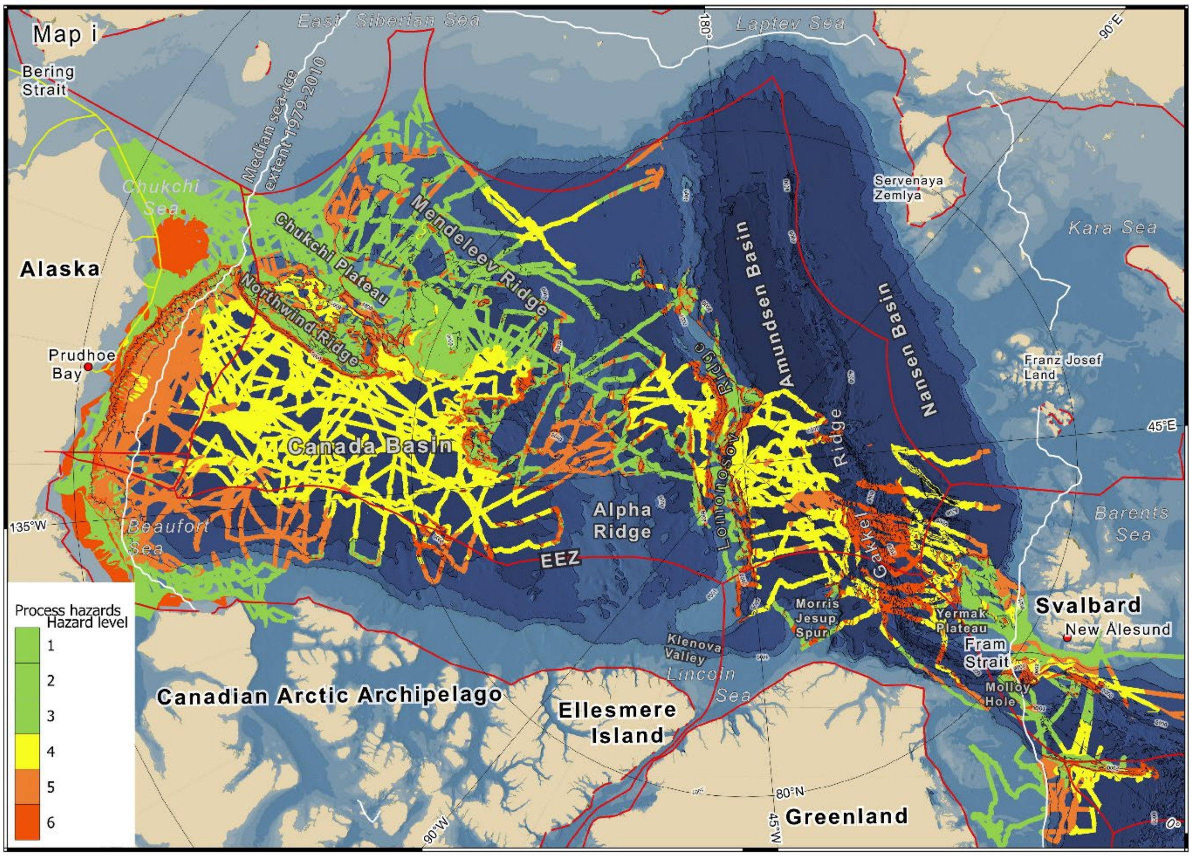

Figure 6. Map h: *Geometric hazards inferred from interpretation of sub-bottom profiles.* ***Map i:*** *Process hazards inferred from interpretation of sub-bottom profiles.*

3.1.2 Static hazards:

The main static hazard along the two proposed routes (R1/2 and R3) are caused primarily along bedrock escarpments and erosional seabeds with relatively steep and narrow slopes of the northern Yermak Plateau and western continental shelf of Svalbard (Fig. 5). In addition, the ancient glacial scours on the Yermak Plateau make the seafloor partly rough (Fig. 8). Furthermore, the cable will have to pass across the pronounced Molloy Fracture Zone, which implies a depth change of ~400 m over ~4000 m (Fig. 8)

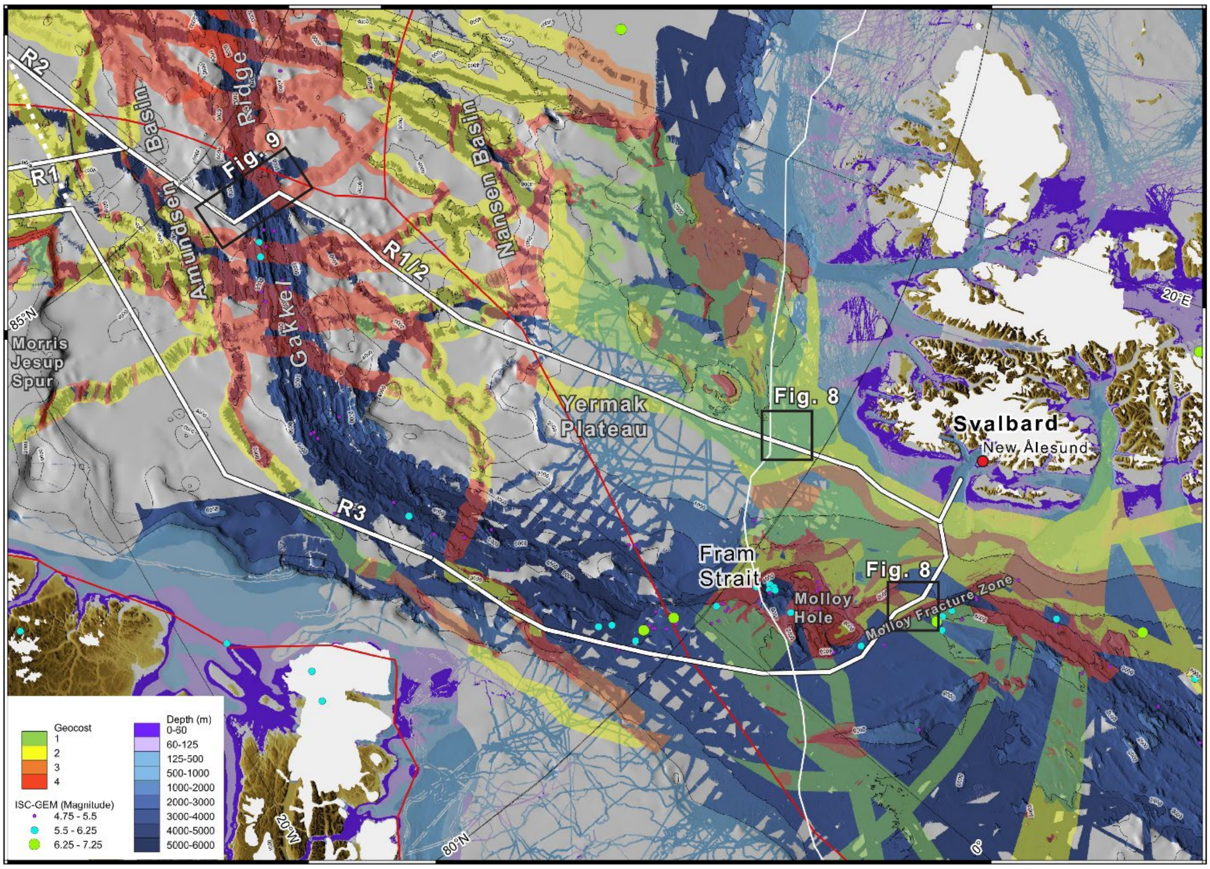

Figure 7. *Map showing two optional cable routes starting outside of New Ålesund. The map displays the results of the geocost analysis, generalized deepest depth of modern iceberg scouring (125 m around Svalbard) and recorded seismic events, which together with seafloor slope and roughness have guided the route selection. The bathymetry in the grey areas is poorly mapped and based on interpolation using single soundings or digitized contours from published charts [Jakobsson et al., 2020].*

3.2 Nansen Basin – Gakkel Ridge – Amundsen Basin

3.2.1 Dynamic hazards:

The dynamic hazards in the Nansen Basin are difficult to fully evaluate with available geophysical data as the area is sparsely mapped. Nonetheless, available data show that the Nansen Basin floor is characterised by hemipelagites and turbidites from the surrounding bathymetric highs. Turbidity current ages are unknown but are likely related to sediment input and mass transport processes along the adjacent margins, which likely were most frequent during glaciation of the shelves [*Ingólfsson and Landvik*, 2013; *Jakobsson et al.*, 2014; *Svendsen et al.*, 2004]. The sub-bottom profiles interpreted in this work show a well stratified sub-bottom stratigraphy and smooth seafloor over a flat abyssal plain (Appendix 1). As we approach the Gakkel Ridge, the seafloor becomes rougher. Sub-bottom seismic profiles in this region are generally of poor quality, primarily attributed to harsh sea-ice conditions when acquired. Most icebreaker expeditions traversing the Nansen Basin prioritize swift passage to other regions for primary data acquisition, which impact data quality due to heavy icebreaking.

The Gakkel Ridge poses significant dynamic hazards as it is a tectonically active zone with ongoing seafloor spreading [*Cochran et al.*, 2003] and rough bottom morphology [*AMORE Shipboard Scientific Parties et al.*, 2001]. Numerous earthquakes are focused to the Gakkel Ridge rift valley where several active volcanoes have been mapped and explosive eruptions have been demonstrated to occur [*Edwards et al.*, 2001; *Pontbriand et al.*, 2012; *Sohn et al.*, 2008]. In addition to these dynamic hazards, there are risks for mass wasting, given the deep and steep valleys in the rift valley. The proposed cable route (R1/2) crosses the rift valley at a location where it reaches a depth of about 4250 m although the bathymetry there is somewhat less dramatic compared with other locations (Fig. 9).

The Amundsen Basin is similar to the Nansen Basin with smooth seafloor and well stratified sub-bottom stratigraphy over the flat deep areas showing no major indications of modern dynamic hazards. However, mass wasting from the slopes of the Lomonosov Ridge do occur [*Kristoffersen et al.*, 2007], generating turbidity currents causing deposition of turbidites as identified in shallow sediment cores from Amundsen Basin [*Svindland and Vorren*, 2002]. Sediment conduits in Amundsen Basin have been identified, e.g. the NP-28 Channel at base of Lomonosov Ridge [*Boggild and Mosher*, 2021; *Kristoffersen et al.*, 2004] and newly identified conduits in data from the *Oden* SAS2021 expedition analyzed in this work (Appendix 1). Cable Routes 1 and 2 crossing the Lomonosov Ridge will have to pass the NP-28 channel. It should be noted that R3 across the Fram Strait could connect to R1/R2, which continues outside of the EEZ from about 85°50 N, as indicated in Figure 7.

3.2.2 Static hazards:

The static hazards in this geographic region is clearly dominated by the Gakkel Ridge and its rough morphology. The ridge was mapped with multibeam during the Arctic Mid-Ocean Ridge Expedition (AMORE) expedition with USCGC Healy and RV Polarstern [*AMORE Shipboard Scientific Parties et al.*, 2001], implying a well portrayed seafloor. The adjacent Amundsen and Nansen basins are characterized by a smooth and flat seafloor once away from the Gakkel and Lomonosov ridges. However, these basins are only sparsely mapped, and judging from available multibeam transects the rough bottom topography as seen across the Gakkel Ridge may be more widely distributed into the basins than apparent in present IBCAO maps.

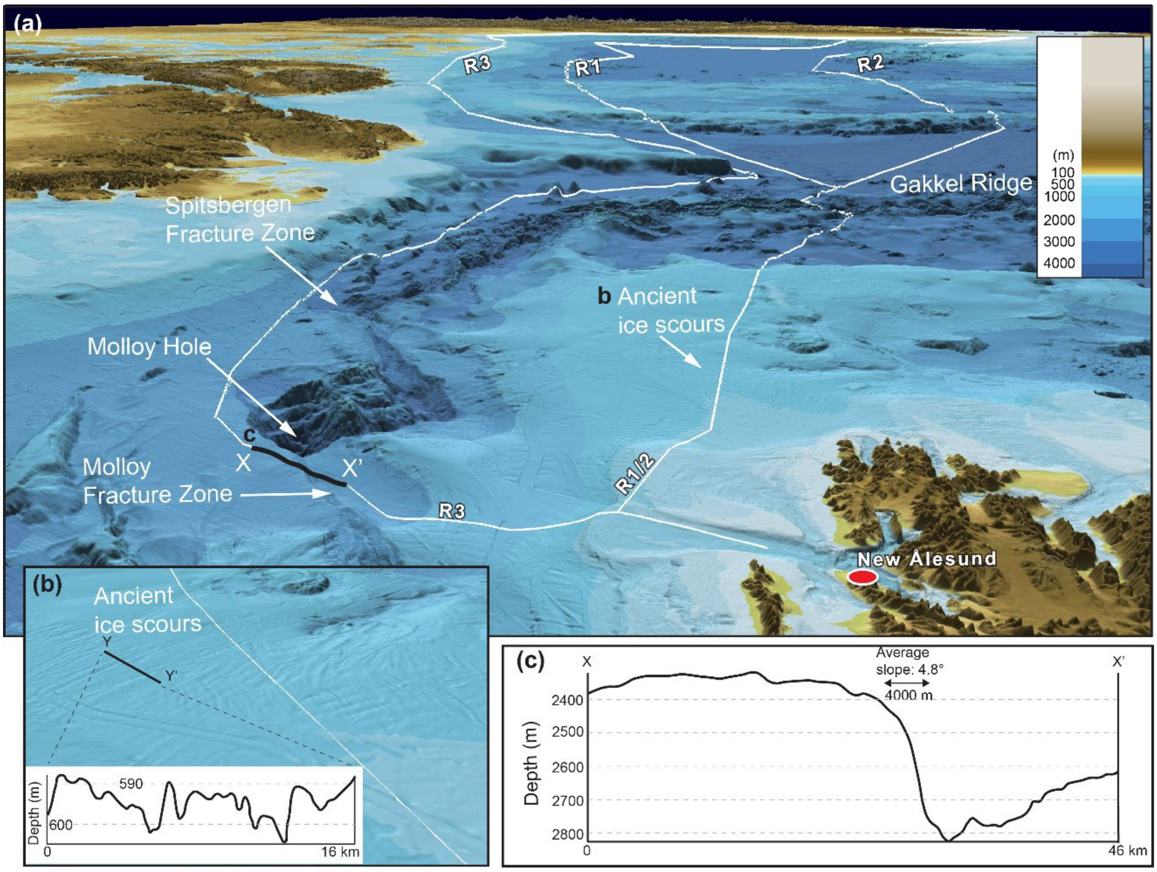

Figure 8. (a) *3D view showing the two main options for the cable route to continue from New Ålesund.* ***(b)*** *Ancient ice scours on the Yermak Plateau.* ***(c)*** *Bathymetric profile across the Molloy Fracture Zone.*

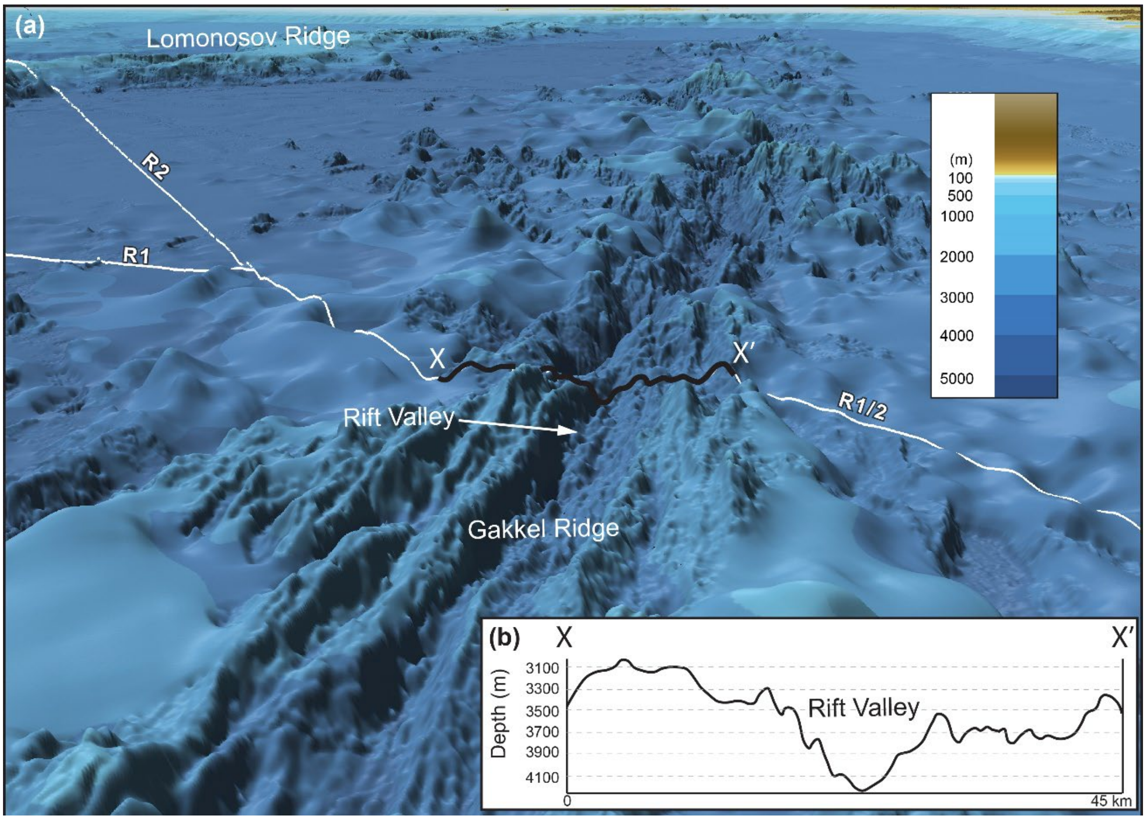

Figure 9. (a) *3D view showing the Gakkel Ridge in the vicinity of cable Route 2.* ***(b)*** *Bathymetric profile along the cable route where it crosses the Gakkel Ridge rift valley.*

3.3 Klenova Valley-Lomonosov Ridge-Alpha Ridge

Cable routes R1 and R2 traverse the complex seafloor morphology of the Alpha and Lomonosov ridges while R3 runs across these ridges' extensions from the shelves of northern Greenland and northern Canada. R4 deviates from R2 to subsequently traverse the Alpha Ridge. There is a large gap in available data about seabed conditions north of Ellesmere Island and Greenland where accumulation of thick sea-ice has historically prevented access by research icebreakers (Figs. 4, 10). Expected seabed conditions in these areas are therefore mostly speculative and need further mapping to confirm. Despite this, some predictions can be made based on data coverage from surrounding areas.

Locations for crossings of Lomonosov Ridge (R1 and R2) were searched for to minimize geometric and dynamic hazards (Fig. 11). However, it should be noted that the bathymetry of the Lomonosov Ridge is not mapped in sufficient detail with multibeam methods to find a suitable passage based on bottom morphology; additional geophysical surveys would be required. R2 avoids both the EEZ of Greenland/Denmark and the most difficult sea-ice conditions north of Greenland and Ellesmere Island (Fig. 12). The southernmost R3 lacks data coverage in these areas. R4 takes the shortest route to Bering Strait by diverting from R2 in the Makarov Basin.

3.3.1 Dynamic Hazards:

Submarine landslides and debrites are mapped in many locations along the crests of Alpha Ridge and Lomonosov Ridge. Along Lomonosov Ridge, submarine landslides are most common along its shoulders and flanks. Failure age estimates range from Pliocene or older, to Quaternary debrites related to grounding of ice-shelves [*Kristoffersen et al.*, 2007; *Pérez et al.*, 2020; *Schlager et al.*, 2021; *Stein et al.*, 2016]. Submarine landslides formed by slope failure processes (rather than glacial processes) are likely the result of triggering by seismicity and may have failed along weak layers in the subsurface (Kristoffersen et al., 2007; Schlager et al., 2021). Routes 1, 2 or 4 do not cross any known submarine landslides along the ridge, however incomplete data coverage does not preclude their existence in these areas.

Multibeam bathymetry and geophysical data along the crest of Alpha Ridge indicate a vast area (>90,000 km^2) characterized by large-scale evidence of mass wasting and submarine landslides [*Boggild et al.*, 2020; *Kristoffersen et al.*, 2008]. Data from icebreaker expeditions only image the northwestern part of these features, however ice-island data acquired in the 1960's from drifting ice-camp T3 suggest that most of the crest of Alpha Ridge, including towards its extension from the shelf of Ellesmere Island, is characterized by submarine landslides at or near the seafloor [*Hall*, 1979; *Kristoffersen et al.*, 2008]. This area of deformed seabed is crossed by Routes 1 and 2 and likely consists of a complex seabed morphology formed by multiple episodes of failure [*Boggild et al.*, 2020]. Recurrence intervals of these failures are poorly constrained due to a lack of dated, or dateable, material from these features. Thus, failure ages may therefore be hundreds of thousands of years apart, presumably triggered by past ground accelerations which (so far) are mostly absent from the modern observational record of seismic activity [*Kristoffersen et al.*, 2008].

There are no data available to evaluate dynamic hazards adjacent to the shelf north of Greenland and Ellesmere Island. It is likely, however, that the seafloor geology in this area is similar to other recently glaciated margins typically characterized by deposition of glacimarine sediments and glacial outwash. Dynamic processes may, for example, include contour currents driven by the flow of deep-water masses [*Björk et al.*, 2010]. Additional geophysical and geological data in these areas would be necessary to understand potential dynamic hazards.

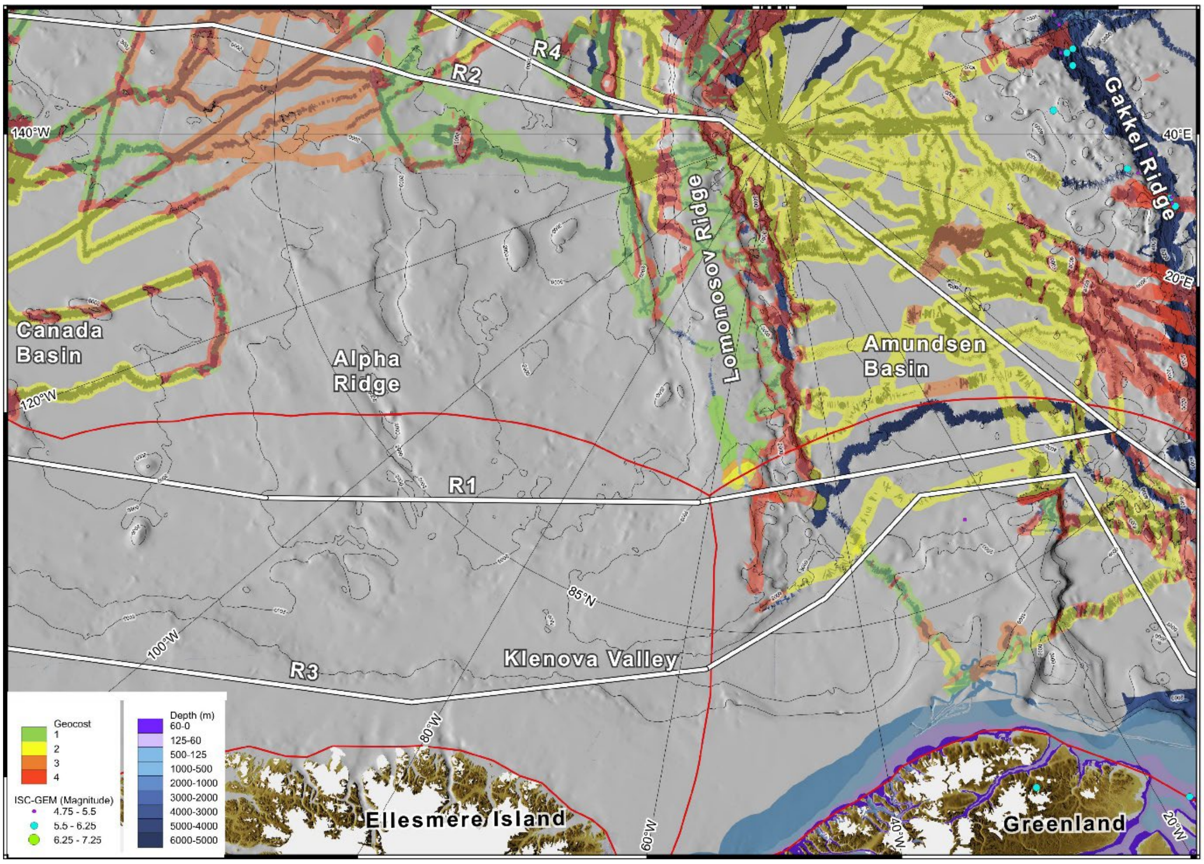

Figure 10. *Map showing Routes 1-4 crossing the Amundsen Basin and Lomonosov Ridge, or through Klenova Valley, to further extend into the Amerasian side of the Arctic Ocean. The map displays the results of the geocost analysis, generalized deepest depth of modern iceberg scouring (60 m along the coast of Canadian Arctic Archipelago) and recorded seismic events, which together with seafloor slope and roughness have guided the route selection. The bathymetry in the grey areas is poorly mapped and based on interpolation using single soundings or digitized contours from published charts [Jakobsson et al., 2020]. This shows that the Alpha Ridge area is virtually unmapped using multibeam bathymetry or sub-bottom profilers.*

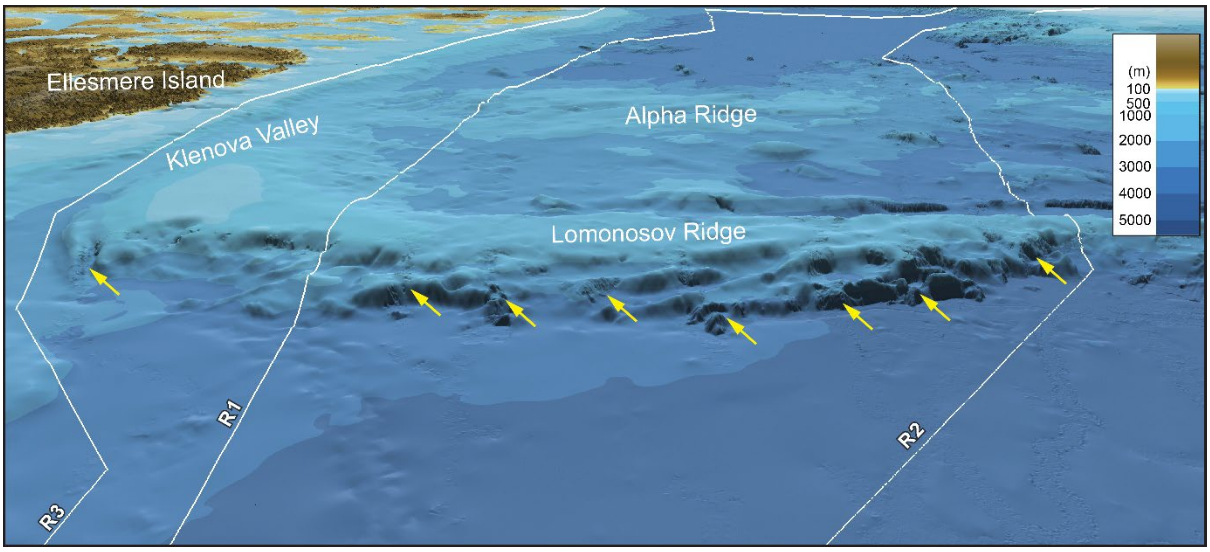

Figure 11. *3D view showing the Lomonosov Ridge from the Amundsen Basin side, with the three Cable Routes 1-3 shown. The yellow arrows indicated where multibeam bathymetry was acquired along transects across the ridge during the LOMROG Expeditions with icebreaker Oden 2007, 2009 and 2012 [Jakobsson et al., 2008; Marcussen and LOMROG II Scientific Party, 2011; Marcussen and LOMROG III Scientific Party, 2012].*

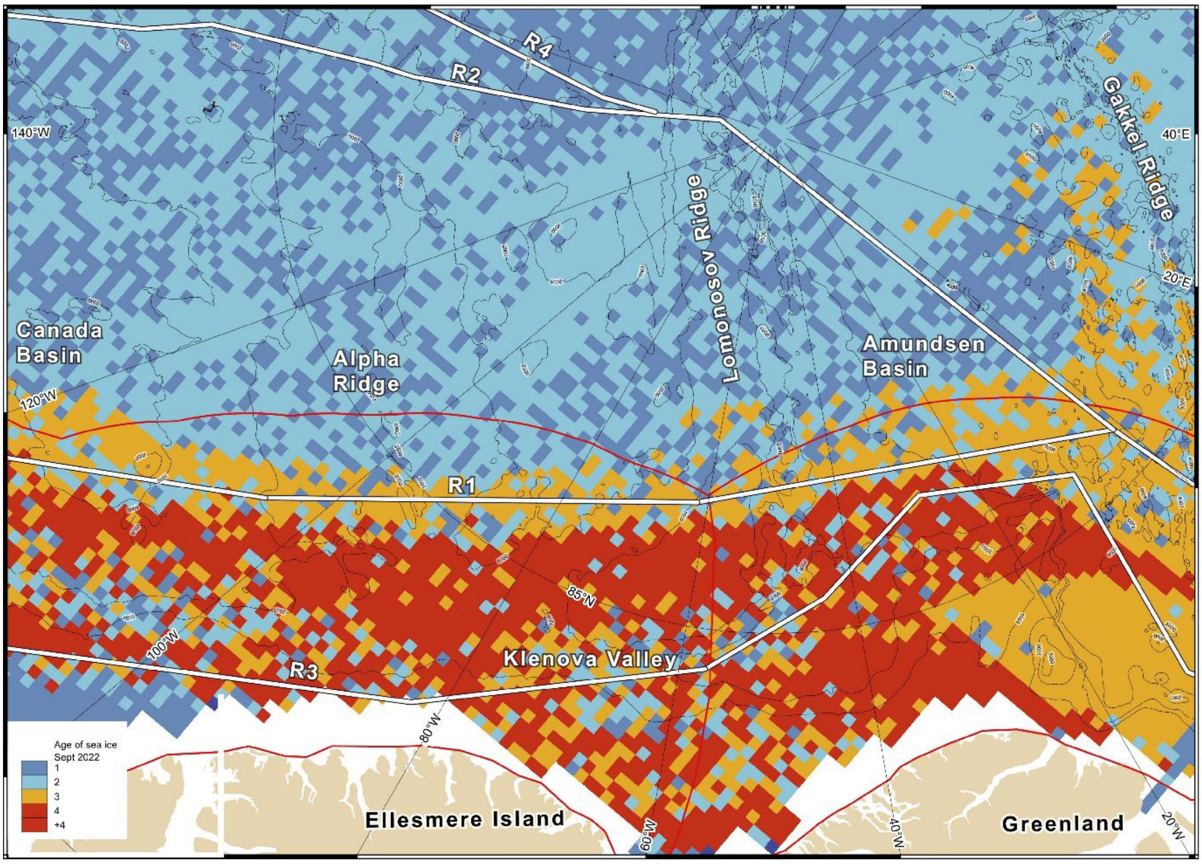

Figure 12. *Yearly sea-ice age for the first week in September 2022 (EASE-Grid Version 4, National Snow and Ice Data Center: https://nsidc.org/data/nsidc-0611/versions/4). The age of sea ice provides a measure of the difficulty for icebreaker operations. Multiyear sea ice is a greater challenge to operate in compared with first year ice. The pattern with the oldest sea ice north of Greenland and Ellesmere Island is reoccurring year by year and is clearly reflected in the sparse data available from these areas.*

3.3.2 Static hazards:

Static hazards along seafloor elevations in the central Arctic principally relate to (a) high slope angles encountered along the flanks of bedrock escarpments, and (b) rough seabed resulting from glacial processes and mass wasting (Fig. 5, Appendix 1). Relict landforms relating to ice grounding along the crest of Lomonosov Ridge, for instance, are found along the seafloor down to a depth of ~1000 m and include megascale glacial lineations, pits and iceberg scours (further described in Appendix 2). Route 1 passes Lomonosov Ridge in one of these areas characterized by ice shelf grounding [*Jakobsson et al.*, 2016], however lack of data precludes an assessment of seafloor roughness. Other complex seabed morphologies related to submarine landslides along Routes 1 and 2 include scarps, ridges and troughs resulting from mass failure processes along Alpha Ridge [*Boggild et al.*, 2020; *Schlager et al.*, 2021].

3.4 Canada Basin and Nautilus Basin cable routes

Due to the large sizes of the Canada Basin and adjoined Nautilus Basin, the cable routes may traverse from north to south and relevant hazards vary according to position in these basins. The four cable routes presented here pass through the shelf (R3), slope and deep basin (R1,R2,R4). Geohazard considerations for these regions are therefore considered separately.

3.4.1 Shelf hazards

3.4.1.1 Dynamic hazards:

Route 3 follows the southeastern shelves of the Canada Basin (CAA shelf, Beaufort Shelf and Alaskan Shelf). Principal dynamic hazards considered along this route relate to (a) potential for ice scouring along shallow seabed (additional information is found in Appendix 2); (b) seabed erosion at the shelf edge, and (c) a suite of dynamic processes related to subsea permafrost and fluid escape located in the Beaufort Sea.

Recent ice scouring within this route is found in areas shallower than 60 m, most of which occurs at depths between 5 and 30 m [*S Blasco et al.*, 2013]. Due to the shallow bathymetry of the Beaufort Shelf and the shelf of northern Alaska, the 60 m isobath nearly reaches the shelf break in several segments along Route 3. This includes the eastern and western margins of the Beaufort Shelf (centered on longitudes approx. 130° W and 137° W, respectively) and the shelf north of Prudhoe Bay, Alaska (approx. 149° W) (Fig. 13). In these areas, recently scoured seabed may be difficult to avoid by cable placement. Route 3, for instance, is pushed close to the edge across these shallow segments of the shelf (Fig. 13). An example of this risk was demonstrated in June 2023, when grounding of sea ice along the seafloor north of Prudhoe Bay in 28 m water depth resulted in a fault in the Quintillion subsea cable [*Quintillion*, 2023], causing a service outage lasting three months. This cable was reportedly buried at a depth of 4 m beneath the seafloor prior to being damaged [*Quintillion*, 2023].

Outer shelf and shelf edge geohazards of the Beaufort Sea are well-described by a number of authors [*S Blasco et al.*, 2013; *King et al.*, 2017; *Charles K. Paull et al.*, 2022; *Woodworth-Lynas et al.*, 2016], and relate to current dynamics as well as subsurface processes. Seabed erosion and current-swept bathymetry along the shelf edge is a result of episodic erosion by currents [*King et al.*, 2017]. The shelf break is also marked by a band of disturbed seafloor characterized by marine pingos, pingo-like features (PLFs), ridges, trenches, and collapse features [*S Blasco et al.*, 2013; *King et al.*, 2017; *Charles K. Paull et al.*, 2022; *Saint-Ange et al.*, 2014]. This distinctive terrain is a result of ongoing dynamic processes relating to a subsurface wedge of subsea permafrost outcropping along the shelf edge; in this area freezing and melting/decay of ice within seafloor sediments produces both positive growth features (e.g., marine pingos) and thermokarst collapse features (e.g., craters, scarps, debris).

Repeat surveying of disturbed seafloor at the shelf edge confirms it is a result of modern processes that produce substantial seabed change up to several tens of meters on yearly timescales (Paull et al., 2022); such seabed changes would therefore pose a hazard to any cables crossing these areas and would be best avoided. The band of seafloor that includes the densest distribution of these features follows the strike of the eastern Beaufort Shelf break and turning landward where it meets shelf-crossing Amundsen and MacKenzie troughs [*King et al.*, 2017]. Width of the disturbed seabed varies from less than 1 km in some areas to 10-12 km at its widest [*King et al.*, 2017]. Gaps or pinching out of this zone would offer best locations for cable route crossings to mitigate risk. Similar PLFs, fluid escape features, mud volcanos and moats also occur as isolated features or clusters throughout the Beaufort Shelf [*K A Blasco et al.*, 2010; *Charles K. Paull et al.*, 2007]. The dimensions of these features can be on the order of 1-2 km in diameter or smaller and may be accompanied by efflux of fluid or gas.

3.4.1.2 Static hazards:

Geometric hazards along the shelf are principally due to extensively scoured seabed. Shallower than 60 m, scour incurred during current high-stand conditions are a result of sea-ice pressure ridges and calved glacial ice.

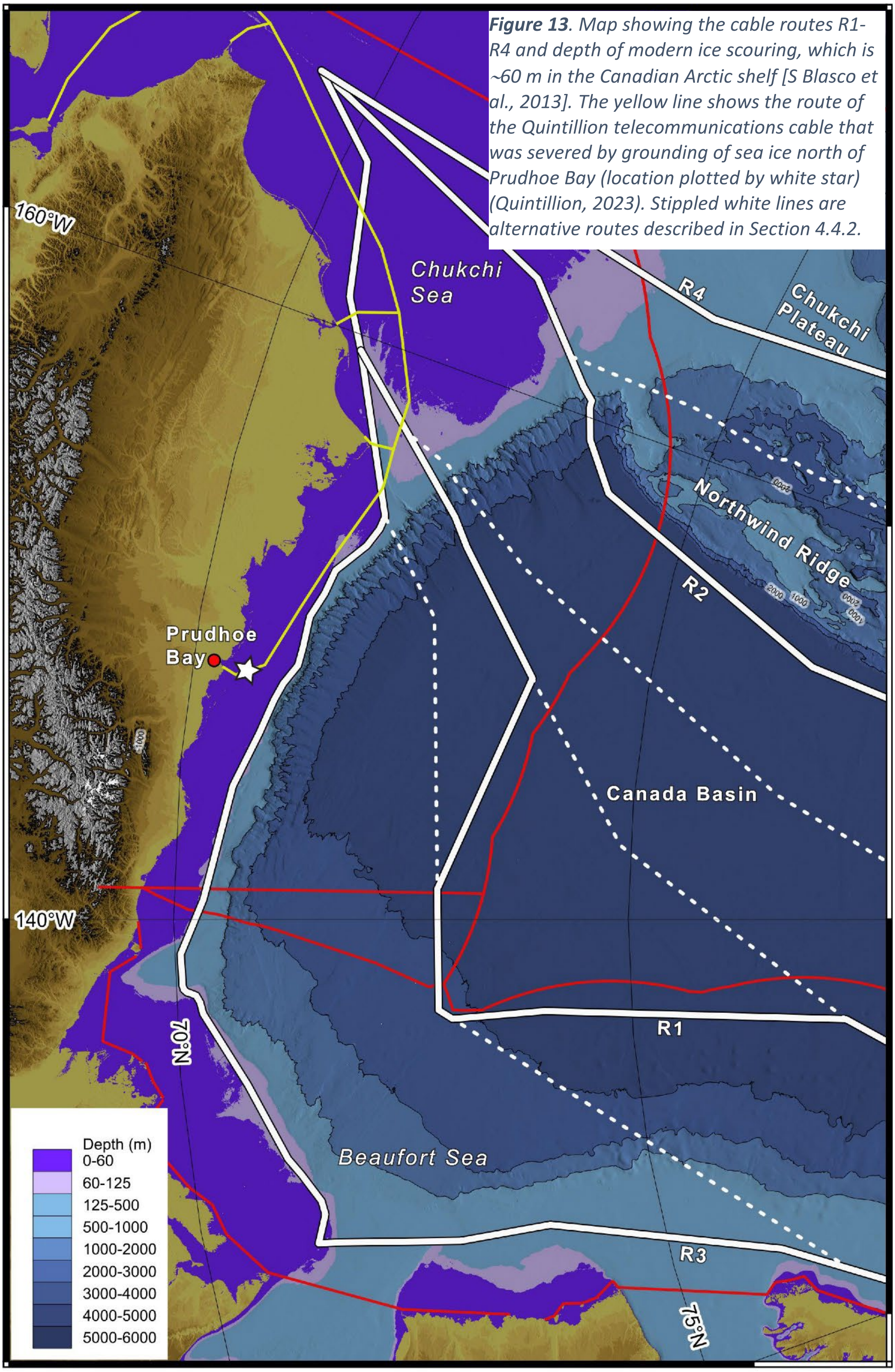

***Figure 13**. Map showing the cable routes R1-R4 and depth of modern ice scouring, which is ~60 m in the Canadian Arctic shelf [S Blasco et al., 2013]. The yellow line shows the route of the Quintillion telecommunications cable that was severed by grounding of sea ice north of Prudhoe Bay (location plotted by white star) (Quintillion, 2023). Stippled white lines are alternative routes described in Section 4.4.2.*

The northern Canadian shelf areas seaward of the Canadian Arctic Archipelago (CAA) are mostly deeper than 60 m, and are characterized by a suite of relict (ancient) scoured features down to depths of ~400 m, produced by grounded ice sheets and iceberg scouring during the last glacial cycle [*Engels et al.*, 2008; *Jakobsson et al.*, 2014; *Michael Riedel et al.*, 2021]. Scoured seabed in these areas therefore includes tills, subglacial landforms, iceberg turbates, and possibly exposures of glacially eroded bedrock. Diamict sediments in these areas are likely to be geotechnically diverse and may contain sediments up to boulder size, like surficial till).

In the Beaufort Sea segment, rough seabed hazards may be encountered related to outcropping or shallow subsea permafrost. Heterogeneous geotechnical characteristics of sediments and shallow subsea permafrost in these areas may also be a consideration for cable burial.

3.4.2 Slope hazards

3.4.2.1 Dynamic hazards:

Routes 1 and 2 cross slopes of the eastern Canada Basin (including slopes of the Canadian Arctic Archipelago, Beaufort Sea, and northern Alaska). In these areas, principal dynamic hazards relate to gravitational processes of mass transport and gravity currents within sediment conduits.

The majority of the southern and eastern slopes of Canada Basin are characterized by mass transport deposits (MTDs) in the shallow subsurface or at the seabed. These features vary in age from older glacial debris flows seaward of former ice streams, to recent Holocene submarine landslides to the south. Ages of individual slope failures are only estimated for a few locations along the Beaufort Sea upper slope, however sub-bottom profiles show MTDs that are both buried and at the seafloor, suggesting possibility of recurring failure. Preconditioning factors for slope failure in the Beaufort Sea likely relate to rapid sedimentation, fluid flow, mud volcanism and subsea permafrost processes along shelf break and upper slope [*Gwiazda et al.*, 2018; *C. K. Paull et al.*, 2021; *Saint-Ange et al.*, 2014]. Gas hydrates also underpin large areas of the Alaskan slope and continue beneath the eastern Beaufort Shelf [*Kayen and Lee*, 1991; *M. Riedel et al.*, 2017; *Ruppel and Hart*, 2022]. Raising ocean temperatures may exacerbate slope instability in some slope areas due to increased potential for dissociation of gas hydrates [*Phrampus et al.*, 2014].

Comprehensively studied MTDs are located on the Beaufort Sea slope with extensive evidence of mass wasting from deglaciation through the late Holocene [*Cameron and King*, 2019; *Michael Riedel et al.*, 2021]. Recurrence intervals of Beaufort Sea failures suggest ongoing failure risk with centennial (100 yr) to millennial (1000 yr) timescales [*Cameron and King*, 2019; *Michael Riedel et al.*, 2021]. The most recent failures in this area are thought to be only several hundred years old [*Cameron and King*, 2019; *Cameron et al.*, 2017; *C. K. Paull et al.*, 2021]. Volumes of sediments displaced during these failure events are significant (totalling >100 km^3) and could easily break cables located downslope or within the slide area itself.

Glacial debris flows seaward of glacial troughs along the CAA margin (such as M'Clure and Amundsen troughs) relate to glacial erosion and redeposition at the shelf edge by former ice streams forming trough fans [*Boggild et al.*, 2018; *Niessen et al.*, 2010]. Due to lack of data coverage and sediment core information in these areas, present-day slope stability of these deposits is not well known. Evidence from other formerly glaciated margins suggest post-glacial failures along similar trough mouth fans may occur [*Renata G. Lucchi et al.*, 2012]. Such examples are thought to arise from differing geotechnical characteristics of glacial debris flows and other intervening glacimarine and plumite sediments [*J. Llopart et al.*, 2015; *Jaume Llopart et al.*, 2019].

Deep ocean and gravity currents within sediment conduits are another possible risk to submarine cables along the slopes. Sediment conduits such as narrow channels and canyonized morphology along the Alaskan slope may be focal points for gravity currents [*Luneva et al.*, 2020]. High angle slopes in these areas are likely also prone to failure as evidenced by scarps in bathymetry and blocky mass transport deposits on the slope [*Kayen and Lee*, 1991]. Slope and deep-sea channels originating along the CAA margin also extend westward into Canada Basin [*Boggild et al.*, 2018]. Redistribution of sediment by currents is obvious along the lower slopes of both the Canadian and Alaskan margins of Canada Basin where there is evidence of sediment drifts and low-amplitude bedforms [*David C. Mosher and Boggild*, 2021].

3.4.2.2 Static hazards

Static hazards mostly relate to complex seabed resulting from submarine landslides and mass failure scarps along the route. Canyonized morphology of the northern Alaska slope presents complex bathymetry with numerous high-angle escarpments along canyon walls that could pose geometric risks to submarine cables.

Sparse data coverage along the northern Canadian Arctic Archipelago due to ice coverage means that little is known about the geometric hazards in these areas beyond what is expected from regional compilations and comparative morphology of the neighboring margin. Bedrock ridges such as Sever Spur and seamounts in Stefansson Basin, for example, are characterized by high seafloor gradients in these areas.

3.4.3 Basin hazards

3.4.3.1 Dynamic hazards:

Cables laid through the western side of Canada Basin would be laid across flat basin floor turbidites, low-amplitude contourite/turbidite features, and occasional submarine channels [*Grantz et al.*, 1996; *David C. Mosher and Boggild*, 2021]. Turbidites in the western part of the Canada Basin Abyssal Plain are thought to be the distal result of mass failures (e.g., submarine landslides) from the surrounding margins which transformed into unconfined turbidity currents [*Campbell and Clark*, 1977; *Grantz et al.*, 1996]. Turbidites dated in a core located in the south of the basin have an average recurrence interval of approximately 2000 years with the two most recent turbidites dated younger than 3.6 ka [*Grantz et al.*, 1996].

3.4.3.2 Static hazards:

The deep basin is effectively flat to undulating with only minor gradients and present little to no geometric hazards.

4. Sea ice and alternative cable routes

4.2.1 Sea ice

The Arctic Ocean is experiencing a sea-ice reduction trend attributed to climate warming, with the minimum ice-extent in September declining in area with ~13 % per decade [*Yadav et al.*, 2020] (Fig. 14). The multiyear sea ice, i.e. the ice surviving more than one season, has also been greatly reduced over time [*Babb et al.*, 2023] (Fig. 14). As previously mentioned, the age of sea ice serves as an indication on how difficult it is to carry out icebreaker operations, with older multiyear ice making a greater challenge. The area north of Greenland and CAA remains, however, dominated by multiyear ice, even if a large reduction has taken place over time also here (Fig. 14). A few icebreaker expeditions have reached these difficult areas, for example the two expeditions with Swedish Icebreaker (IB) *Oden*, i.e. LOMROG 2007 [*Jakobsson et al.*, 2008] and SAS2021. During LOMROG 2007, IB *Oden* was accompanied by the Russian nuclear icebreaker *50 years of Victory*.

Route R2 is directed to steer clear of the most severe sea-ice conditions, which implies running partly outside of any countries EEZs in parts of the Amundsen Basin and the Canada Basin (Fig. 15). From a logistical point of view, this R2 is preferable.

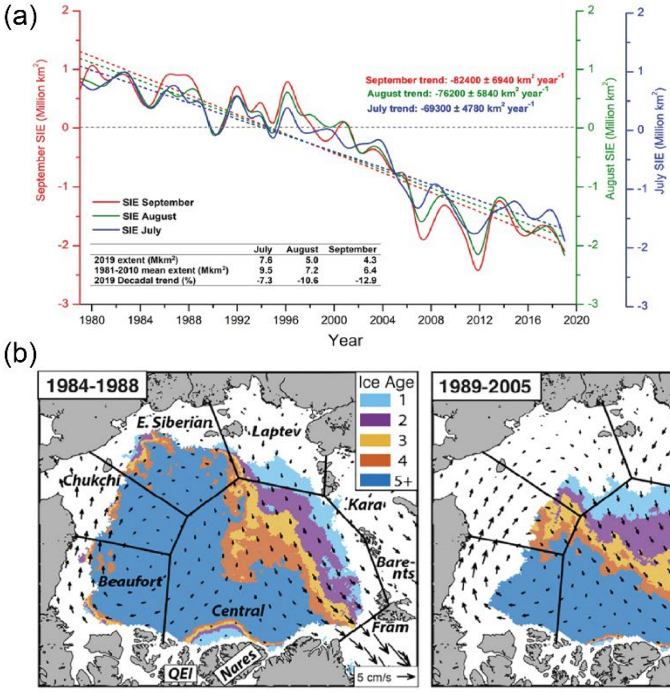

	July	August	September
2019 extent (Mkm²)	7.6	5.0	4.3
1981-2010 mean extent (Mkm²)	9.5	7.2	6.4
2019 Decadal trend (%)	-7.3	-10.6	-12.9

***Figure 14. (a)** Sea-ice area anomaly for the summer months July, August and September relative to 1981-2010, analyzed by National Snow and Ice Data center (NSIDC). The figure is modified from Yadav et al. [2020]. **(b)** Maps of mean sea-ice age during yearly minima (September month) for three time periods. Maps are from Babb et al. [2023].*

4.4.2 Alternative routes

Two main alternative options for routes crossing from western Canada Basin towards the Bering Strait are considered: (a) R1x and R1y, through the flat western side of the Canada Basin abyssal plain, and (b) R2x through the Northwind Basin of the Chukchi Borderlands (Figs. 1, 15 and 16). In addition, we have outlined options for moving over from one route to another, from east to west: R3-2, R1-2, R3-1, R1-3 (Figs. 1, 15, 16).

4.4.2.1 Dynamic and geometric hazards:

R1x and R1y pass through the outer slope and abyssal plain of the Canada Basin beyond the EEZ. These routes therefore pass seaward of most mapped submarine landslides located along the slope, and instead encounter flat to undulating seabed dominated by turbidites, deep sea channels and drift features [Boggild et al., 2018]. Dynamic hazards in this area principally relate to Holocene turbidites in the deep Canada Basin which have recurrence intervals of approximately 2000 years (see Section 3.4.3).

An alternative route R2x diverting from R2 passes through the Northwind Basin, crossing steep flanks of the Chukchi Borderland instead of the Canada Basin abyssal plain. Once inside the Northwind Basin, the cable route passes flat seabed characterized by hemipelagites and turbidites. Turbidites in the Northwind Basin are mostly derived from glacial debris flows extending northward from the formerly glaciated Chukchi margin [*Dove et al.*, 2014]. Glacial debris flows underpin much of the southern slope. Little is known turbidite recurrence in Northwind Basin, however it is possible that they are less recent than Holocene turbidites in the Canada Basin since glacial processes no longer border the margin. Despite this, steep flanks and debris flows along route may present dynamic and geometric hazards. Fluid expulsion features (pockmarks) are also found in several areas throughout the Chukchi Borderland, and may be found areas that are yet to be mapped.

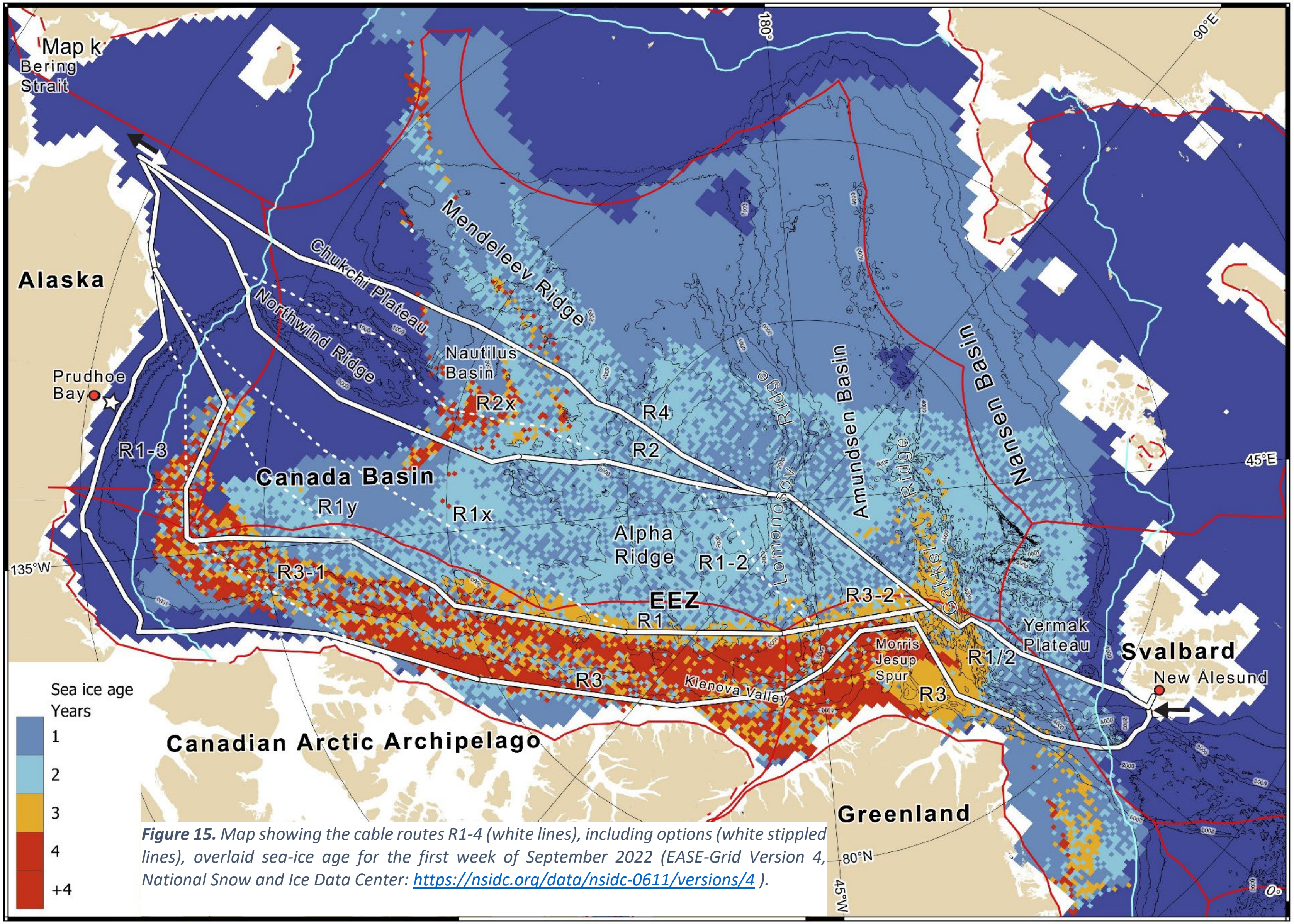

Figure 15. Map showing the cable routes R1-4 (white lines), including options (white stippled lines), overlaid sea-ice age for the first week of September 2022 (EASE-Grid Version 4, National Snow and Ice Data Center: https://nsidc.org/data/nsidc-0611/versions/4).

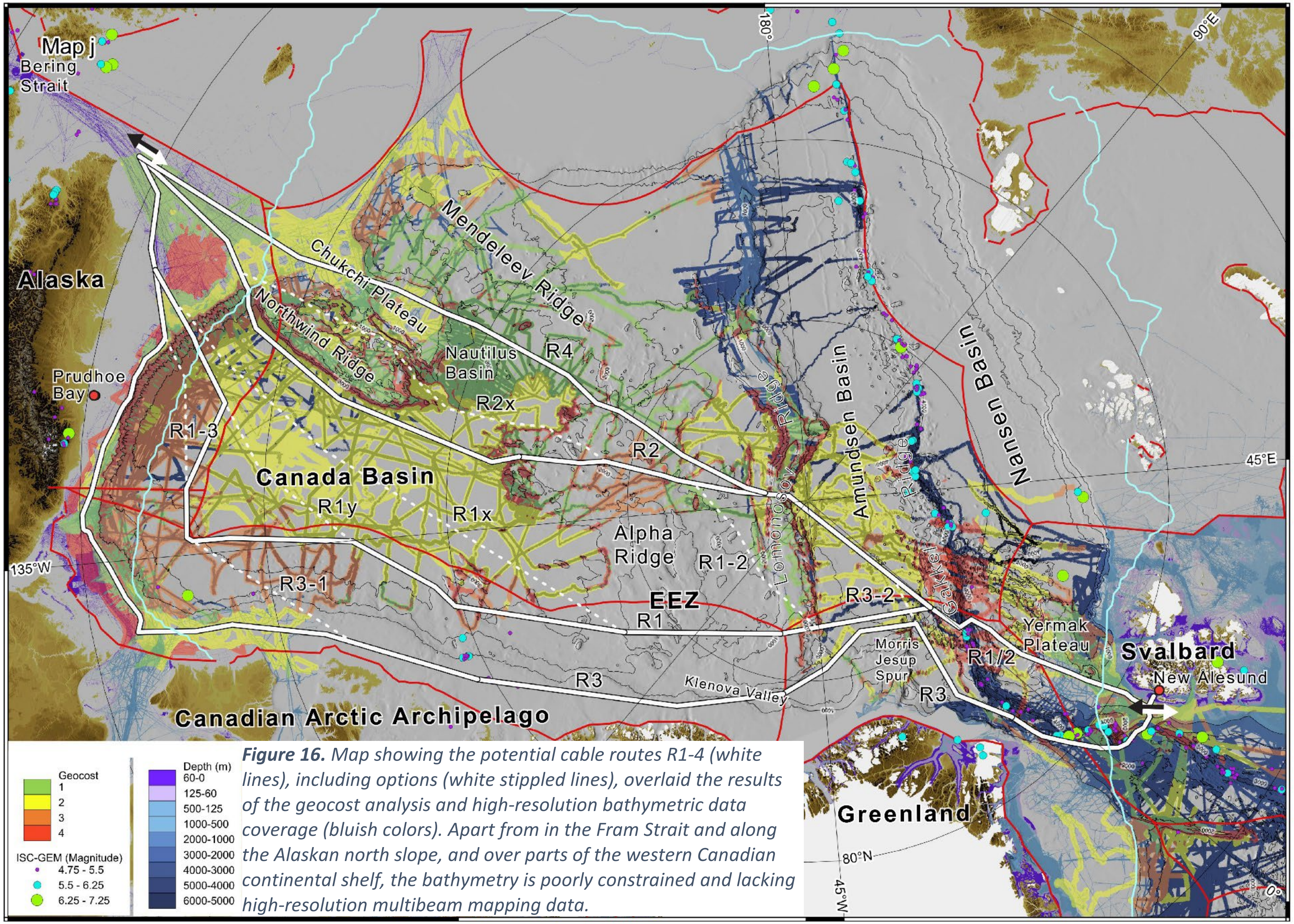

Figure 16. *Map showing the potential cable routes R1-4 (white lines), including options (white stippled lines), overlaid the results of the geocost analysis and high-resolution bathymetric data coverage (bluish colors). Apart from in the Fram Strait and along the Alaskan north slope, and over parts of the western Canadian continental shelf, the bathymetry is poorly constrained and lacking high-resolution multibeam mapping data.*

5. Summary, conclusions and required additional mapping

- Four main cable-route alternatives (R1-R4) are considered, accounting for various factors such as geometric and dynamic geohazards, sea-ice conditions, and the extents of the EEZs of Svalbard/Norway, Greenland/Denmark, Canada, and the United States.
    - R1: Inside EEZs
    - R2: Partly outside EEZs to avoid difficult sea-ice conditions
    - R3: Inside EEZs, including the shallow continental shelf of the Canadian Arctic Archipelago and northern Alaska.
    - R4: Diverting from R2 to take the shortest route towards Bering Strait.
- Optional routes are outlined, including crossings between the main routes R1-R3 or deviations along stretches from them.
- Considerable geohazards are unavoidable along all of the routes, for example:
    - Crossing areas with seismic activities such as the Gakkel Ridge (R1/2), the Fram Strait across the Molloy Fracture Zone (R3), and close to the Spitsbergen Fracture Zone (R3).
    - Crossing considerable seafloor topography, such as the Lomonosov Ridge (R2) or the Alpha Ridge (R1 and R2).
    - All routes include stretches along the shallow continental shelves where ice scouring poses a geohazard. This hazard is minimized by running the cable routes below the general reach of modern ice drafts.
- Considerable logistical challenges are highlighted for R1 and R3 due to multiyear sea-ice conditions, while R2 is designed to circumnavigate the worst multiyear sea ice.
- R2 is the preferred route if the longest possible path in deep water is preferred. It is overall the second shortest and the logistical challenges concerning geophysical mapping and cable installation in heavy sea-ice are less than that for the R1 and R3.
- R4 is the “low cost” route from both a distance and sea-ice perspective.
- R1 however is the preferred option if the cable route must be located inside the EEZs.
- Moving from R3 over to either R1 or R2 along R3-2 is an option if the Gakkel Ridge is evaluated as being associated with too large geohazards.
- The poorly mapped seafloor in the central Arctic Ocean, except for some areas like the northern Alaskan slope, adjacent deep abyssal plain, and the Fram Strait, implies that more mapping than just along the proposed cable routes is most likely needed to ensure optimal seafloor conditions for a cable installation. For example, across the Lomonosov and Alpha ridges where the bathymetry is largely unmapped.
- Coring for geotechnical studies of seafloor sediment should be added along with the reconnaissance mapping, especially where cable burial is considered, such as route segments on the shelves.
- Geophysical mapping should at the minimum include multibeam bathymetry and sub-bottom profiling considering the variable seabed geology in the central Arctic Ocean.

Table 6 provides a summary of the lengths of the main routes (R1-R4), alternative routes, and includes a rough estimation of survey speeds, considering sea-ice conditions. Survey speed, in this context, refers to the speed the icebreaker can maintain while acquiring valuable geophysical mapping data. It is important to note that this is distinct from the maximum speed an icebreaker can achieve while breaking ice. Estimating survey speed is challenging due to the variability in sea-ice conditions from year to year, and no remote sensing method offers a comprehensive overview. In this analysis, we utilized the estimated sea-ice age from September 2022 to provide insights into the icebreaking conditions that influence survey speeds.

For the acquisition of high-quality geophysical mapping data in the central Arctic Ocean, a two-ship operation is deemed most effective. One ship supports the other by breaking ice in the front allowing for relatively clear water for the geophysical data acquisition. Few complete transects across the entire central Arctic Ocean have been undertaken. In 2005, IB *Oden* and USCGC *Healy* completed a transect, supporting each other from a rendezvous point on the Alpha Ridge (Figure 17). USCGC *Healy* took 49 days to travel from Barrow, Alaska, to the Yermak Plateau, while IB *Oden* used 35 days to journey from the northern Alaskan shelf to Longyearbyen, Svalbard (Figure 17). Considering these transit times, the information presented in Table 6, and the additional mapping required over complex areas such as ridges, we propose two expeditions, each lasting between about 45 and 55 days depending on the route selection, to map the optimal cable route across the central Arctic Ocean. Both expeditions should operate as two-ship operations, and each ship should be equipped with state-of-the-art multibeam and sub-bottom profilers. The icebreaking capacity must be sufficient for operations in the central Arctic Ocean sea ice.

Table 6. *Distances along R1-R4 and alternative routes and estimated survey speeds considering ice conditions, here based on sea-ice ages for September 2022. The estimated days are excluding station work, and additional mapping that may bee required over complex areas such as crossing the Lomonosov and Alpha ridges.*

Route	Segment	Sea-ice age	Distance (nmi)	Speed	Estimated full days
R1/2 - R2	Start - 1	0-1	106	5	1
	1-2	1-2	246	4	3
	2-3	3	83	2	2
	3-4	1-3	943	2	20
	4-End	0-1	661	5	6
			2039		**32**
R1/2 - R1	Start - 1	0-1	106	5	1
	1-2	1-2	246	4	3
	2-3	3	83	2	2
	3-4	3-4	1508	2	32
	4-End	0-1	439	5	4
			2382		**42**
R3	Start - 1	1-2	128	5	2
	1-2	1-2	172	4	2
	2-3	3	235	2	5
	3-4	3-4	1036	2	22
	4-End	0-1	1160	5	10
			2731		**41**
R1/2- R2 - R4	Start - 1	0-1	106	5	1
	1-2	1-2	246	4	3
	2-3	3	83	2	2
	3-4	1-3	667	2	14
	4-End	0-1	519	5	5
			1621		**25**
Alternative legs					
R3-2	Start - End	3	84	2	2
R1-2	Start - End	1-3	319	2	7
R2x	Start - 1	1-3	302	2	7
	1-End	0-1	403	5	4
R1x	Start - 1	1-3	550	2	12

	1 - End	0-1	357	5	3
R1y	Start - 1	1-3	190	2	4
	1 - End	0-1	126	5	2
R3-1	Start - End	3-4	305	2	7
R1-3	Start - 1	2-4	84	2	2
	1-End	0-1	169	5	2

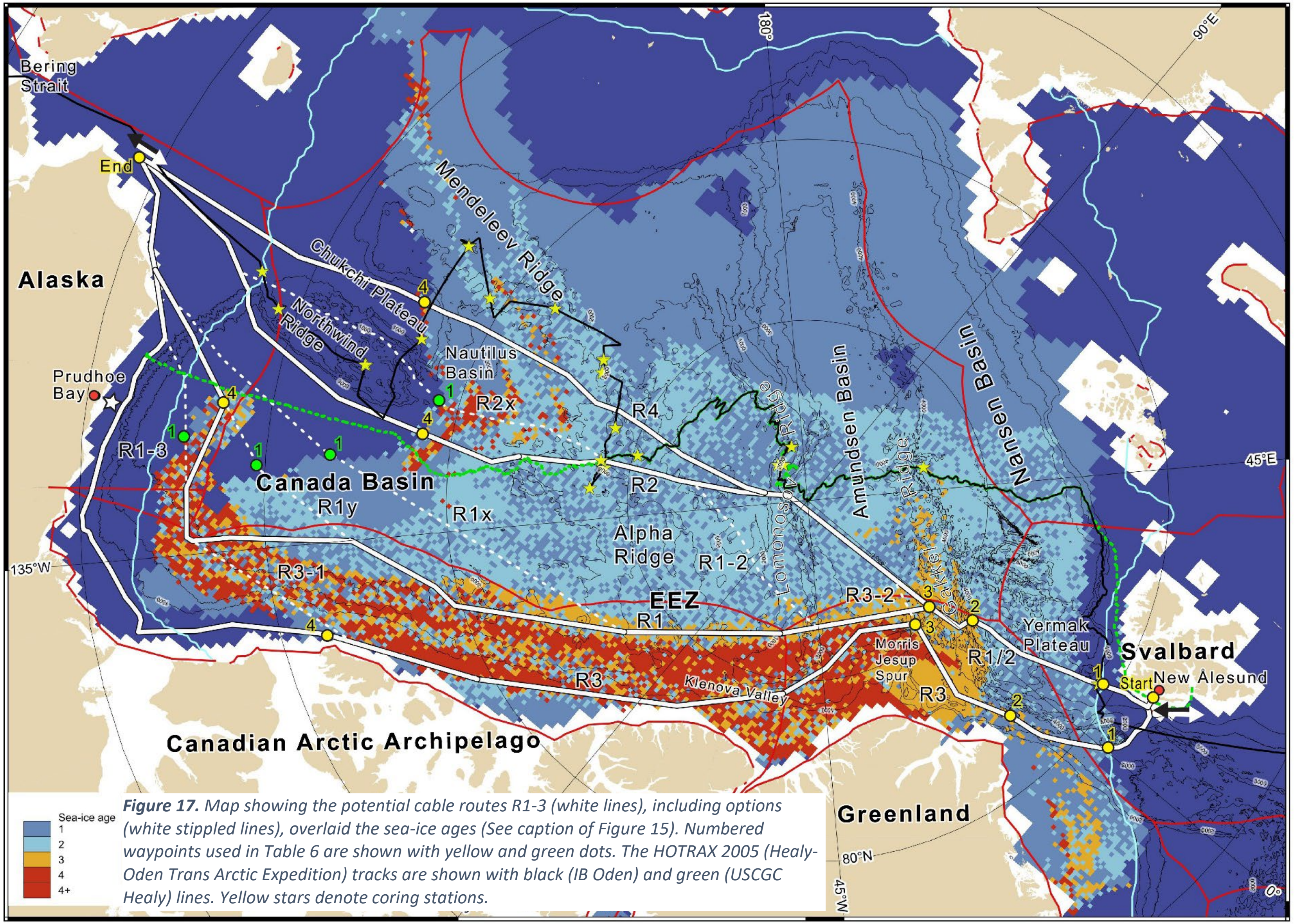

__Figure 17.__ Map showing the potential cable routes R1-3 (white lines), including options (white stippled lines), overlaid the sea-ice ages (See caption of Figure 15). Numbered waypoints used in Table 6 are shown with yellow and green dots. The HOTRAX 2005 (Healy-Oden Trans Arctic Expedition) tracks are shown with black (IB Oden) and green (USCGC Healy) lines. Yellow stars denote coring stations.

6. References

American Bureau of Shipping (2016), Guidance Notes on Subsea Pipeline Route Determination*Rep.*, 1-56 pp, American Bureau of Shipping, Houston, TX, USA.

AMORE Shipboard Scientific Parties, P. Michael, J. Thiede, W. Jokat, E. Weigelt, O. Ritzmann, K. Lehnert, M. C. Schmidt-Aursch, and J. Standish (2001), Results of the Arctic Mid-Ocean Ridge Expedition -AMORE 2001- Seafloor spreading at the top of the World, *Interridge News, Vol. 10(2)*, 57-60.

Babb, D. G., R. J. Galley, S. Kirillov, J. C. Landy, S. E. L. Howell, J. C. Stroeve, W. Meier, J. K. Ehn, and D. G. Barber (2023), The Stepwise Reduction of Multiyear Sea Ice Area in the Arctic Ocean Since 1980, *Journal of Geophysical Research: Oceans*, *128*(10), e2023JC020157, doi:https://doi.org/10.1029/2023JC020157.

Björk, G., et al. (2010), Flow of Canadian basin deep water in the Western Eurasian Basin of the Arctic Ocean, *Deep Sea Research Part I: Oceanographic Research Papers*, *57*(4), 577-586, doi:10.1016/j.dsr.2010.01.006.

Blasco, K. A., S. M. Blasco, R. Bennett, B. MacLean, W. A. Rainey, and E. H. Davies (2010), Seabed geologic features and processes and their relationship with fluid seeps and the benthic environment in the Northwest Passage*Rep.*, 1-58 pp.

Blasco, S., et al. (2013), 2010 State of Knowledge: Beaufort Sea Seabed Geohazards Associated with Offshore Hydrocarbon Development; Geological Survey of Canada*Rep.*, 1-340 pp, Geological Survey of Canada.

Boggild, K., and M. Jakobsson (in prep), Seabed conditions in the central Arctic Ocean with regards to submarine cables: examples from subbottom profiler data*Rep.*

Boggild, K., and D. C. Mosher (2021), Turbidity currents at polar latitudes: A case study of NP-28 channel in the Amundsen Basin, Arctic Ocean, *Marine Geology*, *440*, 106571, doi:https://doi.org/10.1016/j.margeo.2021.106571.

Boggild, K., D. C. Mosher, C. Gebhardt, K. E. Baldwin, and J. van der Krogt (2023), Mapping surficial geology in the Artic Ocean, in *The 9th International Conference on Arctic Margins (ICAM 9)* edited by M.-C. Williamson, B. M. Saumur, A. M. Savoie and N. Bingham-Koslowski, Geological Survey of Canada, Open File

Boggild, K., D. C. Mosher, C. Gebhardt, M. Jakobsson, L. A. Mayer, K. A. Hogan, and D. Dove (2018), Surficial geology of the Amerasian Basin from subbottom profiler data (No. 8465)*Rep.*

Boggild, K., D. C. Mosher, P. Travaglini, C. Gebhardt, and L. Mayer (2020), Mass wasting on Alpha Ridge in the Arctic Ocean: new insights from multibeam bathymetry and sub-bottom profiler data, *Geological Society, London, Special Publications*, *500*(1), 323-340, doi:doi:10.1144/SP500-2019-196.

Bünz, S., S. Polyanov, S. Vadakkepuliyambatta, C. Consolaro, and J. Mienert (2012), Active gas venting through hydrate-bearing sediments on the Vestnesa Ridge, offshore W-Svalbard, *Marine Geology*, *332-334*, 189-197, doi:https://doi.org/10.1016/j.margeo.2012.09.012.

Cameron, G. D. M., and E. L. King (2019), Mass-failure complexes on the central Beaufort Slope, offshore Northwest Territories*Rep.*

Cameron, G. D. M., E. L. King, D. Murray, Z. A. Kuzyk, and S. Blasco (2017), Relative timing of sediment failures within slide-valley complexes in the Kugmallit Fan area of the central Beaufort Slope, offshore Northwest Territories*Rep.*, Geological Survey of Canada.

Campbell, J. S., and D. L. Clark (1977), Pleistocene turbidites of the Canada abyssal plain of the Arctic Ocean, *Journal of Sedimentary Research*, *47*(2), 657-670, doi:10.1306/212f7211-2b24-11d7-8648000102c1865d.

Cochran, J. R., G. J. Kurras, M. H. Edwards, and B. J. Coakley (2003), The Gakkel Ridge: Bathymetry, gravity anomalies, and crustal accretion at extremely slow spreading rates, *Journal of Geophysical Research: Solid Earth*, *108*(B2), doi:https://doi.org/10.1029/2002JB001830.

Damuth, J. E. (1980), Use of high-frequency (3.5–12 kHz) echograms in the study of near-bottom sedimentation processes in the deep-sea: A review, *Marine Geology*, *38*(1), 51-75, doi:https://doi.org/10.1016/0025-3227(80)90051-1.

Dove, D., L. Polyak, and B. Coakley (2014), Widespread, multi-source glacial erosion on the Chukchi margin, Arctic Ocean, *Quaternary Science Reviews*, *92*(0), 112-122, doi:http://dx.doi.org/10.1016/j.quascirev.2013.07.016.

Dowdeswell, J. A., and C. F. Forsberg (1992), The size and frequency of icebergs and bergy bits derived from tidewater glaciers in Kongsfjorden, northwest Spitsbergen, *Polar Research*, *11*(2), 81-91, doi:https://doi.org/10.1111/j.1751-8369.1992.tb00414.x.

Dowdeswell, J. A., et al. (2010), High-resolution geophysical observations from the Yermak Plateau and northern Svalbard margin: implications for ice-sheet grounding and deep-keeled icebergs, *Quaternary Science Reviews*, *29*(25-26), 3518-3531, doi:2075/10.1016/j.quascirev.2010.06.002.

Edwards, M. H., G. J. Kurras, M. Tolstoy, D. R. Bohnenstiehl, B. J. Coakley, and J. R. Cochran (2001), Evidence of recent volcanic activity on the ultraslow-spreading Gakkel ridge, *Nature*, *409*(6822), 808-812, doi:10.1038/35057258.

Elger, J., C. Berndt, L. Rüpke, S. Krastel, F. Gross, and W. H. Geissler (2018), Submarine slope failures due to pipe structure formation, *Nature Communications*, *9*(1), 715, doi:10.1038/s41467-018-03176-1.

Engels, J. L., M. H. Edwards, L. Polyak, and P. D. Johnson (2008), Seafloor evidence for ice shelf flow across the Alaska–Beaufort margin of the Arctic Ocean, *Earth Surface Processes and Landforms*, *32*(14), 1-17, doi:10.1002/esp.1601.

Gatter, R., M. A. Clare, J. Kuhlmann, and K. Huhn (2021), Characterisation of weak layers, physical controls on their global distribution and their role in submarine landslide formation, *Earth-Science Reviews*, *223*, 103845, doi:https://doi.org/10.1016/j.earscirev.2021.103845.

Grantz, A., R. L. Phillips, M. W. Mullen, S. W. Starratt, G. A. Jones, A. S. Naidu, and B. P. Finney (1996), Character, paleoenvironment, rate of accumulation, and evidence for seismic triggering of Holocene turbidites, Canada Abyssal Plain, Arctic Ocean, *Marine Geology*, *133*(1 - 2), 51 - 73.

Gwiazda, R., C. K. Paull, S. R. Dallimore, H. Melling, Y. K. Jin, J. K. Hong, M. Riedel, E. Lundsten, K. Anderson, and K. Conway (2018), Freshwater Seepage Into Sediments of the Shelf, Shelf Edge, and Continental Slope of the Canadian Beaufort Sea, *Geochemistry, Geophysics, Geosystems*, *19*(9), 3039-3055, doi:https://doi.org/10.1029/2018GC007623.

Hall, J. K. (1979), Sediment Waves and Other Evidence of Paleo-Bottom Currents at two Locations in the Deep Arctic Ocean, *Sedimentary Geology*, *23*, 269-299.

Hesse, R., S. Khodabakhsh, I. Klaucke, and W. B. F. Ryan (1997), Asymmetrical turbid surface-plume deposition near ice-outlets of the Pleistocene Laurentide ice sheet in the Labrador Sea, *Geo-Marine Letters*, *17*(3), 179-187, doi:10.1007/s003670050024.

Hustoft, S., S. Bünz, J. Mienert, and S. Chand (2009), Gas hydrate reservoir and active methane-venting province in sediments on < 20 Ma young oceanic crust in the Fram Strait, offshore NW-Svalbard, *Earth and Planetary Science Letters*, *284*(1–2), 12-24, doi:http://dx.doi.org/10.1016/j.epsl.2009.03.038.

Ingólfsson, Ó., and J. Y. Landvik (2013), The Svalbard–Barents Sea ice-sheet – Historical, current and future perspectives, *Quaternary Science Reviews*, *64*(0), 33-60, doi:http://dx.doi.org/10.1016/j.quascirev.2012.11.034.

Iqbal, M., F. Sattar, and M. Nawaz (2006), *Planning a Least Cost Gas Pipeline Route A GIS & SDSS Integration Approach*, 126-130 pp., doi:10.1109/ICAST.2006.313812.

Jakobsson, M., et al. (2014), Arctic Ocean glacial history, *Quaternary Science Reviews*, *92*(0), 40-67, doi:10.1016/j.quascirev.2013.07.033.

Jakobsson , M., C. Marcussen, and S. P. LOMROG (2008), Lomonosov Ridge Off Greenland 2007 (LOMROG) - Cruise Report, *Cruise report Rep.*, 122 pp, Geological Survey of Denmark and Greenland, Copenhagen.

Jakobsson, M., et al. (2020), The International Bathymetric Chart of the Arctic Ocean Version 4.0, *Scientific Data*, *7*(1), 176, doi:10.1038/s41597-020-0520-9.

Jakobsson, M., et al. (2016), Evidence for an ice shelf covering the central Arctic Ocean during the penultimate glaciation, *Nature Communication*, *7*, 1-10, doi:10.1038/ncomms10365.

Kayen, R. E., and H. J. Lee (1991), Pleistocene slope instability of gas hydrate-laden sediment on the Beaufort sea margin, *Marine Geotechnology*, *10*(1-2), 125-141, doi:10.1080/10641199109379886.

King, E. L., et al. (2017), A belt of seabed erosion along the Beaufort Sea margin, offshore Northwest Territories, governed by Holocene evolution of the Beaufort Shelf-Break Jet; geological evidence, current measurements, and initial oceanographic modelling*Rep.*

Kristoffersen, Y., B. J. Coakley, J. K. Hall, and M. Edwards (2007), Mass wasting on the submarine Lomonosov Ridge, central Arctic Ocean, *Marine Geology*, *243*(1-4), 132-142.

Kristoffersen, Y., et al. (2008), Extensive local seabed disturbance, erosion and mass wasting on Alpha Ridge, central Arctic Ocean: Possible evidence for an extra-terrestrial impact?, *Norsk Geologisk Tidsskrift*, *88*, 313-320.

Kristoffersen, Y., M. Y. Sorokin, W. Jokat, and O. Svendsen (2004), A submarine fan in the Amundsen Basin, Arctic Ocean, *Marine Geology*, *204*(3-4), 317-324.

Llopart, J., R. Urgeles, A. Camerlenghi, R. G. Lucchi, M. Rebesco, and B. De Mol (2015), Late Quaternary development of the Storfjorden and Kveithola Trough Mouth Fans, northwestern Barents Sea, *Quaternary Science Reviews*, *129*, 68-84, doi:https://doi.org/10.1016/j.quascirev.2015.10.002.

Llopart, J., R. Urgeles, C. F. Forsberg, A. Camerlenghi, M. Vanneste, M. Rebesco, R. G. Lucchi, D. C. Rüther, and H. Lantzsch (2019), Fluid flow and pore pressure development throughout the evolution of a trough mouth fan, western Barents Sea, *Basin Research*, *31*(3), 487-513, doi:https://doi.org/10.1111/bre.12331.

Lucchi, R. G., et al. (2013), Postglacial sedimentary processes on the Storfjorden and Kveithola trough mouth fans: Significance of extreme glacimarine sedimentation, *Global and Planetary Change*, *111*, 309-326, doi:https://doi.org/10.1016/j.gloplacha.2013.10.008.

Lucchi, R. G., M. T. Pedrosa, A. Camerlenghi, R. Urgeles, B. De Mol, and M. Rebesco (2012), Recent Submarine Landslides on the Continental Slope of Storfjorden and Kveithola Trough-Mouth Fans (North West Barents Sea), Springer Netherlands, Dordrecht.

Luneva, M. V., V. V. Ivanov, F. Tuzov, Y. Aksenov, J. D. Harle, S. Kelly, and J. T. Holt (2020), Hotspots of Dense Water Cascading in the Arctic Ocean: Implications for the Pacific Water Pathways, *Journal of Geophysical Research: Oceans*, *125*(10), e2020JC016044, doi:https://doi.org/10.1029/2020JC016044.

Marcussen, C., and LOMROG II Scientific Party (2011), Lomonosov Ridge Off Greenland 2009 (LOMROG II) - Cruise Report*Rep.*, 151 pp, Geological Survey of Denmark and Greenland, Ministry of Climate and Energy.

Marcussen, C., and LOMROG III Scientific Party (2012), Lomonosov Ridge Off Greenland 2012 (LOMROG III) - Cruise Report*Rep.*, 220 pp, Geological Survey of Denmark and Greenland, Geological Survey of Denmark and Greenland, Ministry of Climate and Energy.

Mosher, D. C., and K. Boggild (2021), Impact of bottom currents on deep water sedimentary processes of Canada Basin, Arctic Ocean, *Earth and Planetary Science Letters*, *569*, 117067, doi:https://doi.org/10.1016/j.epsl.2021.117067.

Mosher, D. C., R. C. Courtney, M. Jakobsson, C. Gebhardt, and L. Mayer (2015), Mapping the Surficial Geology of the Arctic Ocean: A Layer for the IBCAO, paper presented at OTC Arctic Technology Conference.

Niessen, F., J. Matthiessen, and R. Stein (2010), Sedimentary environment and glacial history of the Northwest Passage (Canadian Arctic Archipelago) reconstructed from high-resolution acoustic data, *Polarforschung*, *79*(2), 65-80.

Paull, C. K., et al. (2021), A 100-km wide slump along the upper slope of the Canadian Arctic was likely preconditioned for failure by brackish pore water flushing, *Marine Geology*, *435*, 106453, doi:https://doi.org/10.1016/j.margeo.2021.106453.

Paull, C. K., S. R. Dallimore, Y. K. Jin, D. W. Caress, E. Lundsten, R. Gwiazda, K. Anderson, J. Hughes Clarke, S. Youngblut, and H. Melling (2022), Rapid seafloor changes associated with the degradation of Arctic submarine permafrost, *Proceedings of the National Academy of Sciences*, *119*(12), e2119105119, doi:doi:10.1073/pnas.2119105119.

Paull, C. K., W. Ussler, S. R. Dallimore, S. M. Blasco, T. D. Lorenson, H. Melling, B. E. Medioli, F. M. Nixon, and F. A. McLaughlin (2007), Origin of pingo-like features on the Beaufort Sea shelf and their possible relationship to decomposing methane gas hydrates, *Geophysical Research Letters*, *34*(1), n/a-n/a, doi:10.1029/2006GL027977.

Pérez, L. F., M. Jakobsson, T. Funck, K. J. Andresen, T. Nielsen, M. O'Regan, and F. Mørk (2020), Late Quaternary sedimentary processes in the central Arctic Ocean inferred from geophysical mapping, *Geomorphology*, *369*, 107309, doi:https://doi.org/10.1016/j.geomorph.2020.107309.

Phrampus, B. J., M. J. Hornbach, C. D. Ruppel, and P. E. Hart (2014), Widespread gas hydrate instability on the upper U.S. Beaufort margin, *Journal of Geophysical Research: Solid Earth*, *119*(12), 8594-8609, doi:https://doi.org/10.1002/2014JB011290.

Plaza-Faverola, A., N. Sultan, R. G. Lucchi, N. El bani Altuna, H. Ramachandran, S. Singhroha, F. Cooke, S. Vadakkepuliyambatta, M. M. Ezat, and T. L. Rasmussen (2023), Spatial Changes in Gas Transport and Sediment Stiffness Influenced by Regional Stress: Observations From Piezometer Data Along Vestnesa Ridge, Eastern Fram Strait, *Journal of Geophysical Research: Solid Earth*, *128*(5), e2022JB025868, doi:https://doi.org/10.1029/2022JB025868.

Pontbriand, C. W., S. A. Soule, R. A. Sohn, S. E. Humphris, C. Kunz, H. Singh, K. I. Nakamura, M. Jakobsson, and T. Shank (2012), Effusive and explosive volcanism on the ultraslow-spreading Gakkel Ridge, 85°E, *Geochemistry, Geophysics, Geosystems*, *13*(10), doi:10.1029/2012GC004187.

QGIS Development Team (2023), QGIS Geographic Information System. Open Source Geospatial Foundation Project, edited.

Quintillion, I. (2023), Service Outage Notification, published June 13 2023: https://www.quintillionglobal.com/update-to-service-outage-notification/, edited.

Riedel, M., T. A. Brent, G. Taylor, A. E. Taylor, J. K. Hong, Y. K. Jin, and S. R. Dallimore (2017), Evidence for gas hydrate occurrences in the Canadian Arctic Beaufort Sea within permafrost-associated shelf and deep-water marine environments, *Marine and Petroleum Geology*, *81*, 66-78, doi:https://doi.org/10.1016/j.marpetgeo.2016.12.027.

Riedel, M., S. Dallimore, M. Wamsteeker, G. Taylor, E. L. King, K. M. M. Rohr, J. K. Hong, and Y. K. Jin (2021), Mega-scale glacial lineations formed by ice shelf grounding in the Canadian Beaufort Sea during multiple glaciations, *Earth Surface Processes and Landforms*, *46*(8), 1568-1585, doi:https://doi.org/10.1002/esp.5125.

Ruppel, C. D., and P. E. Hart (2022), Gas Hydrates on Alaskan Marine Margins, in *World Atlas of Submarine Gas Hydrates in Continental Margins*, edited by J. Mienert, C. Berndt, A. M. Tréhu, A. Camerlenghi and C.-S. Liu, pp. 209-223, Springer International Publishing, Cham, doi:10.1007/978-3-030-81186-0_17.

Saint-Ange, F., P. Kuus, S. Blasco, D. J. W. Piper, J. H. Clarke, and K. MacKillop (2014), Multiple failure styles related to shallow gas and fluid venting, upper slope Canadian Beaufort Sea, northern Canada, *Marine Geology*, *355*, 136-149, doi:https://doi.org/10.1016/j.margeo.2014.05.014.

Schlager, U., W. Jokat, E. Weigelt, and C. Gebhardt (2021), Submarine landslides along the Siberian termination of the Lomonosov Ridge, Arctic Ocean, *Geomorphology*, *382*, 107679, doi:https://doi.org/10.1016/j.geomorph.2021.107679.

Sohn, R. A., et al. (2008), Explosive volcanism on the ultraslow-spreading Gakkel Ridge, Arctic Ocean, *Nature*, *453*(26 June), 1236-1238, doi:http://dx.doi.org/10.1038/nature07075.

Stein, R., et al. (2016), Evidence for ice-free summers in the late Miocene central Arctic Ocean, *Nature Communication*, *7*, doi:10.1038/ncomms11148.

Storchak, D. A., D. Di Giacomo, I. Bondár, E. R. Engdahl, J. Harris, W. H. K. Lee, A. Villaseñor, and P. Bormann (2013), Public Release of the ISC–GEM Global Instrumental Earthquake Catalogue (1900–2009), *Seismological Research Letters*, *84*(5), 810-815, doi:10.1785/0220130034.

Svendsen, J. I., et al. (2004), Late Quaternary ice sheet history of northern Eurasia, *Quaternary Science Reviews*, *23*(11-13), 1229-1271, doi:10.1016/j.quascirev.2003.12.008.

Svindland, K. T., and T. O. Vorren (2002), Late Cenozoic sedimenatry environments in the Amundsen Basin, Arctic Ocean, *Marine Geology*, *186*(3 - 4), 541 - 555.

Van der Krogt, J. (2018), Acoustic facies mapping of the Lomonosov Ridge and adjacent basins, in the Arctic Ocean, Utecht University, Utecht, Netherlands.

Wiberg, D. H., H. Haflidason, and J. S. Laberg (2022), An updated Weichselian chronostratigraphic framework of the Kongsfjorden Trough Mouth Fan and its implications for the glacial history of Svalbard, *Boreas*, *51*(3), 667-683, doi:https://doi.org/10.1111/bor.12581.

Woodworth-Lynas, C., S. Blasco, D. Duff, J. Fowler, E. B. Isler, J. Landva, E. Cumming, A. Caines, and C. Smith (2016), Regional assessment of seabed geohazard conditions Canadian Beaufort outer shelf and upper slope - legacy data synthesis: section 2, geophysical and geological data compilation, outer shelf and upper slope southern Beaufort Sea: a handbook of geohazard conditions*Rep.*, Geological Survey of Canada, Ottawa, Ontario

Yadav, J., A. Kumar, and R. Mohan (2020), Dramatic decline of Arctic sea ice linked to global warming, *Natural Hazards*, *103*(2), 2617-2621, doi:10.1007/s11069-020-04064-y.